Journal of Pharmacological and Toxicological Methods 123 (2023) 107281

Contents lists available at ScienceDirect

Journal of Pharmacological and Toxicological Methods

journal homepage: www.elsevier.com/locate/jpharmtox

Comparative assessment of Ca^{2+} oscillations in 2- and 3-dimensional hiPSC derived and isolated cortical neuronal networks

John P. Imredy [a,*], Gautier Roussignol [b], Holly Clouse [a], Giorgia Salvagiotto [c], Ludmilla Mazelin-Winum [b]

[a] In Vitro Safety Pharmacology, Merck & Co., Inc., Rahway, NJ, USA
[b] Preclinical Safety, Sanofi R&D, Montpellier, France
[c] Fujifilm Cellular Dynamics, Inc., Madison, WI, USA

ARTICLE INFO

Keywords:
Calcium
Cortical neuron
hiPSC
In vitro
Methods
Mouse
Networks
Neurons
Neurotoxicity
Safety pharmacology
Seizures

ABSTRACT

Human induced Pluripotent Stem Cell (hiPSC) derived neural cells offer great potential for modelling neurological diseases and toxicities and have found application in drug discovery and toxicology. As part of the European Innovative Medicines Initiative (IMI2) NeuroDeRisk (Neurotoxicity De-Risking in Preclinical Drug Discovery), we here explore the Ca^{2+} oscillation responses of 2D and 3D hiPSC derived neuronal networks of mixed Glutamatergic/GABAergic activity with a compound set encompassing both clinically as well as experimentally determined seizurogenic compounds. Both types of networks are scored against Ca^{2+} responses of a primary mouse cortical neuronal 2D network model serving as an established comparator assay. Parameters of frequency and amplitude of spontaneous global network Ca^{2+} oscillations and the drug-dependent directional changes to these were assessed, and predictivity of seizurogenicity scored using contingency table analysis. In addition, responses between models were compared between both 2D models as well as between 2D and 3D models. Concordance of parameter responses was best between the hiPSC neurospheroid and the mouse primary cortical neuron model (77% for frequency and 65% for amplitude). Decreases in spontaneous Ca^{2+} oscillation frequency and amplitude were found to be the most basic shared determinants of risk of seizurogenicity between the mouse and the neurospheroid model based on testing of clinical compounds with documented seizurogenic activity. Increases in spontaneous Ca^{2+} oscillation frequency were primarily observed with the 2D hIPSC model, though the specificity of this effect to seizurogenic clinical compounds was low (33%), while decreases to spike amplitude in this model were more predictive of seizurogenicity. Overall predictivities of the models were similar, with sensitivity of the assays typically exceeding specificity due to high false positive rates. Higher concordance of the hiPSC 3D model over the 2D model when compared to mouse cortical 2D responses may be the result of both a longer maturation time of the neurospheroid (84–87 days for 3D vs. 22–24 days for 2D maturation) as well as the 3-dimensional nature of network connections established. The simplicity and reproducibility of spontaneous Ca^{2+} oscillation readouts support further investigation of hiPSC derived neuronal sources and their 2- and 3-dimensional networks for neuropharmacological safety screening.

1. Introduction

Induced pluripotent stem cell (iPSC) derived excitable cells have facilitated research on human models of physiological responses of excitable cell systems, including muscle as well as nerve systems. The presence of the human isoforms of receptors makes these models sine qua non the human physiological response especially to pharmacological effects. Recent developments of directed differentiation of hiPSC stem cells to neuronal and glial cells have enabled the investigation of mixtures of these cell types in both 2- and 3-dimensional networks. It has been demonstrated, for example, that hIPSC derived neurons can be directed to dopaminergic, glutamatergic, and GABAergic phenotypes and that combinations of these can reproduce responses of brain regions of similar neuronal and glial cell admixture (Kundu, Boutin, Strong, Voss, & Ferrer, 2022; Slavin et al., 2021; Strong et al., 2022). Specifically, the combination of an excess of glutamatergic with a fractional

* Corresponding author at: Merck & Co., Inc., WP81-2207, 770 Sumneytown Pike, West Point, PA 19486, USA.
E-mail address: john_imredy@merck.com (J.P. Imredy).

https://doi.org/10.1016/j.vascn.2023.107281
Received 16 March 2023; Received in revised form 9 June 2023; Accepted 16 June 2023
Available online 29 June 2023

GABAergic representation has found application in modelling the responses of the cortex (Yokoi, Shigemoto-Kuroda, Matsuda, Odawara, & Suzuki, 2022). Furthermore, addition of astrocytes has improved the formation and synchronization of the functional network (Ishii, Yamamoto, Shoji, Asami, & Kawamata, 2017; Kuijlaars et al., 2016; Odawara, Katoh, Matsuda, & Suzuki, 2016) with the aim of having a model of neuronal responses closely aligned with cortical network function. Especially with regard to the pharmacological induction of seizures, the importance of the role of the cortex as a substrate of seizurogenic activity is elevated.

To accelerate and facilitate drug development the European IMI2 initiative has formed the NeuroDeRisk consortium with the aim to mitigate both neurotoxic and seizurogenic risk of drug candidates. Eighteen groups comprising academic centers, small and medium-sized enterprises, and European Federation of Pharmaceutical Industries and Associations (EFPIA) industry partners participated in this initiative (NeuroDeRisk, 2019). The aim of NeuroDeRisk is to deliver a comprehensive toolbox of tools and data that would make it easier for researchers to assess whether a compound is likely to pose a risk to the brain and nervous system, long before first tests in humans. Part of this aim is the strategic evaluation of readily applied in vitro functional assays and methods utilizing novel cellular models to enhance the ability of the pharmaceutical industry to screen compounds for ictogenic risk (Rockley, Roberts, & Morton, 2019; Shirakawa & Suzuki, 2020). As part of this initiative, the evaluation of commercially available hiPSC derived neuronal models presents itself as a timely opportunity, given the rapidly expanding demonstration of the utility of these cellular models to provide functional insight into congenital epileptic mechanism (Javaid et al., 2022; Nieto-Estevez & Hsieh, 2020; Tidball & Parent, 2016).

Within the NeuroDeRisk functional evaluation of hiPSC derived neuronal models, we evaluated both 2-dimensional (2D) networks as well as 3D neurospheroids composed of a majority glutamatergic neurons with a fraction of GABAergic neurons and astrocytes admixed. In order to assess function globally, averaged network Ca^{2+} oscillations imaged using fluorescent dyes were used as the functional readout. Global Ca^{2+} fluctuations average Ca^{2+} changes spatially across the entire imaged region of interest, thereby losing detailed local information, as would be available with multi-electrode array (MEA) field potential recordings. However, in contrast to MEA, which records action potential spiking of cell bodies at the surface of the network and infers concerted network activity via temporal spike correlation analysis, Ca^{2+} oscillations are a direct measure of the integrated activity of cell bodies, as well as dendritic and synaptic activity not accessible to the planar MEA electrode (Ali & Kwan, 2020). The integrative nature of the Ca^{2+} signal also allows straightforward interpretation of network signals whether they arise from 2- or 3-dimensional cellular networks, as global parameters such as network Ca^{2+} spiking frequencies and amplitudes can be readily compared between models.

2D cultures of isolated primary cortical neurons of neonatal mice were tested alongside the hiPSC models, as an established comparator assay and as a robust reproducible model for study of cortical network formation and subsequent synchronized network Ca^{2+} and MEA spiking activity (Dravid & Murray, 2004; Kamioka, Maeda, Jimbo, Robinson, & Kawana, 1996; Murphy, Blatter, Wier, & Baraban, 1992; Wang & Gruenstein, 1997). Primary cortical neuron 2D networks have been used in assessment of potential neurotoxicity or seizurogenicity of compounds both using multi-electrode array (Bradley, Luithardt, Metea, & Strock, 2018; Strickland, Martin, Richard, Houck, & Shafer, 2018; Tukker, Wijnolts, de Groot, & Westerink, 2020) and Ca^{2+} oscillation assays (Pacico & Meur, 2013; Pacico & Mingorance-Le Meur, 2014; Roussignol et al., 2017). The time course for stabilization of whole network Ca^{2+} spiking activity has been shown to follow predictable timelines, provided isolated neurons are plated at adequate density in multi-well screening plates such as used in standard Ca^{2+} fluorescent reader platforms (Pacico & Mingorance-Le Meur, 2014; Richards, Jack, Platts, & Simpson, 2006).

Unique to the NeuroDeRisk effort was the identification of a set of drugs where seizurogenic risk has been clinically demonstrated via adverse event reporting (Table 1, FAERS Positive). This approach would take advantage of the existing FDA and World Health Organization adverse event databases where adverse events are catalogued according to event reporting criteria and pharmacovigilance guidelines. By focusing on seizures as adverse events the aim was to be more restrictive to a particular functional toxicity rather than general neurotoxicity. FAERS Seizurogenic Positive and comparator drugs lacking seizurogenic adverse events (Table 1, FAERS Negative) were used to assess how neuronal network level Ca^{2+} oscillation parameters may be used to identify risk. Since risk may arise from both on-target effects, such as exaggerated pharmacology, as well as potential off-target or toxic effects of a compound, screening methodologies should be broad enough to detect both types of effects provided large enough concentration ranges are tested. Once risk is identified, the methodology can help identify safety margins or no effect levels. Such insight can then be used as part of an integrated risk-benefit approach involving all aspects of drug pharmacodynamics and pharmcokinetics to assess the safety of a compound.

2. Methods

2.1. Test drug selection criteria

The NeuroDeRisk compound set (Table 1) tested in our studies was selected using a methodology outlined in previous NeuroDeRisk publications, but specifically targeted to identifying seizurogenic adverse events. (Andronis et al., 2020; Bryant et al., 2022). The FAERS positive and negative designation was arrived at using public databases FDA Adverse Event Reporting System (FAERS) and World Health Organization (WHO) pharmacovigilance (VigiBASE) which were queried to identify compounds with seizurogenic adverse events (AE) using Medical Dictionary for Regulatory Activities (MEDRA) terminology under the class 'Nervous System Disorders'. The events were restricted to adult rather than pediatric events (Age $>$ 21 yrs), and adverse events arising from the same indication for which the drug is prescribed were also omitted. Subsequently, a Disproportionality Analysis was applied to the reported events according to established selection criteria (Andronis et al., 2020) after calculation of the Drug/Seizure-AE Proportional Reporting Ratio (PRR) and Information Component (IC) for each drug (Manuscript in preparation). Disproportionality analysis is a statistical method used in pharmacovigilance to evaluate the frequency of adverse events associated with a particular drug. It compares the rate of a specific adverse drug reaction with a specific drug to the rate reported with all other drugs in the FAERS database.

Tool Compounds were selected by EFPIA partners, based on the literature (Bradley et al., 2018; Easter et al., 2009; Gao, Igata, Takeuchi, Sato, & Ikegaya, 2017; Koseki, Deguchi, Yamashita, Miyawaki, & Funabashi, 2014; Kumlien & Lundberg, 2010; Ruffmann, Bogliun, & Beghi, 2006; Winter et al., 2008) and their internal in vitro and in vivo experiments having demonstrated seizure liability of these compounds.

2.2. hiPSC neurospheroid culture

StemoniX® microBrain® 3D Assay-Ready 384 Well Plates were obtained from Stemonix/Vyant (Maple Grove, MN, Cat# BSARX-AA-0384). The neurospheroids have been described previously (Boutin et al., 2022; Sirenko et al., 2019) and are composed of 50% astrocytes and 50% neurons, of which 20% are GABAergic and 80% are glutamatergic. Each round-bottom well (Corning, Cat# 4516) contained a single neurospheroid. The age of the neurospheroids at assay time was 84–87 days post seeding of hiPSC derived neuroprogenitor cells.(Slavin et al., 2021) Upon receipt of the 384-well/neurospheroid plates, media was fully exchanged and thereafter half-well volume changes were performed at regular 2–3 day intervals using the following phenol-red

Table 1
NeuroDeRisk compound set and pharmacology.

Tool drug		FAERS positive for seizurogenicity		FAERS negative	
Compound (Test range)	Pharmacology	Compound (Test range)	Clinical Use	Compound (Test range)	Clinical Use
4-Aminopyridine (0.03–300 μM)	K^+-channel blocker	Amitriptyline (0.03–10 μM)	Antidepressant, Nerve Pain	Azelastine (0.03–100 μM)	Antihistamine (nasal)
Amoxapine (0.03–100 μM)	Antidepressant, Nerve pain	Bupropion (0.05–100 μM)	Antidepressant	Darifenacin (0.01–300 μM)	Bladder relaxant
Bicuculline (0.05–100 μM)	$GABA_A$ receptor antagonist	Clozapine (0.3–100 μM)	Antipsychotic	Imiquimod (0.003–100 μM)	Topical Immune modulator
Chlorpromazine (0.01–300 μM)	D_2 receptor antagonist, antipsychotic	Diphenhydramine (0.3–100 μM)	Antihistamine	Miconazole (0.003–100 μM)	Topical Antifungal
Donepezil (0.01–100 μM)	Cholinesterase inhibitor	Isoniazid (0.05–100 μM)	Antibiotic	Minoxidil (0.01–30 μM)	Vasodilator (topical and oral)
Kainic Acid (0.03–100 μM)	Kainate receptor agonist	Maprotiline (0.05–300 μM)	Antidepressant and anxiolytic	Niacin (0.05–300 μM)	Vitamin B3
Pentylenetetrazol (PTZ) (0.03–6000 μM)	$GABA_A$ receptor antagonist	Mirtazapine (0.05–300 μM)	Antidepressant	Ospemifene (0.01–100 μM)	Treatment of dyspareunia
Picrotoxin (PTX) (0.03–300 μM)	$GABA_A$ receptor antagonist	Paroxetine (0.05–96 μM)	Antidepressant (SSRI)	Roflumilast (0.05–300 μM)	COPD / Asthma
Pilocarpine (0.05–300 μM)	Muscarinic M_3 receptor agonist	Temozolomide (0.3–100 μM)	Chemotherapy for brain cancer	Rosiglitazone (0.009–100 μM)	TypeII diabetes
SNC-80 (0.1–30 μM)	δ-opioid receptor agonist	Theophylline (0.05–100 μM)	Bronchodilator	Valdecoxib (0.3–100 μM)	NSAID
Strychnine (0.1–30 μM)	Glycine receptor antagonist	Tramadol (0.05–300 μM)	Narcotic		
		Venlafaxine (0.05–300 μM)	Antidepressant		

containing media composition, all from Stem Cell Technologies, Vancouver, CA: BrainPhys™ Neuronal Medium (Cat.# 05792, 97% *v*/v), SM1 Supplement (Cat#05792, 2% v/v), and BDNF (Cat# 78005, 20 ng/ml final), GDNF (Cat# 78058, 20 ng/ml final). The media was supplemented with Penicillin-Streptomycin (GE Healthcare Life Sciences Cat#SV30010, 1% v/v). The plates were incubated for two weeks after receipt in a cell culture incubator at 37 °C, 5% CO_2, and ~ 90% humidity.

2.2.1. Ca^{2+} fluorescence assay of neurospheroids in FDSS

Neurospheroids were assayed at two sites, using either the FDSS platform (FDSS μCell, Hamamatsu, Japan) or the FLIPR platform (Molecular Devices, CA) using methods provided by the vendor. On the day of the assay the media was replaced with phenol-red free test media containing BrainPhys™ Neuronal Medium (Stem Cell Tech., Cat.# 05791, 98% v/v), NeuroCult SM1 Supplement (Stem Cell Tech., Cat#05711, 2% v/v), and BDNF (Stem Cell Tech., Cat# 78005, 20 ng/ml final). Three half-replacements/washes of the total well volume of 50 μl were used to ensure that the neurospheroids were not dislodged from the center of the well during media exchange. The plate was then placed back into the incubator. One vial of lyophilized Ca^{2+} imaging dye (Calcium 6 Dye; Molecular Devices, SanJose, CA, Cat. #R8190) was resuspended in 13 ml of test media by repeat trituration to insure complete dissolution of the mixture. A Janus G3 MDT liquid handler was used to aspirate 25 μl (half-well volume) of the media and replace it with 25 μl of the prepared Ca^{2+} dye mixture per well. The plate was then placed back into the incubator for dye loading for a period of 2 h, at which time a 10 min baseline (BL) read of the spontaneous spiking activity of all 384 neurospheroids in the plate was obtained. The plates were imaged in a Hamamatsu FDSS/μCell plate reader heated to a temperature of 37 °C. The site using the FLIPR platform used the identical stocks as used in the FDSS to prepare and test plates at 37 °C in the FLIPR platform according to previously published methods (Sirenko et al., 2019).

The excitation wavelength of 470 nm in the FDSS/μCell was provided by a LED bank (blue), and the emitted light passed through a 540 nm bandpass filter (green). The cooled CCD camera obtained 200 msec exposures every 500 msec, and pixels were binned into 2 × 2 arrays for readout. A total of 1200 frames were obtained over a 10 min continuous reading time. A physical mask was used to limit light collection to the central area of the well where the microBrain® was located at the bottom of the round well. The Ca^{2+} signal was averaged across the masked area and presented as relative fluorescence units for each time/frame during the recording. The Ca^{2+} concentration transient signals over the 10 min period were exported from the FDSS acquisition software and were analyzed for peak counts and peak amplitude changes using Stemonix AnalytiX™ software, then averaged and visualized in Spotfire® (TIBCO®) software.

2.2.2. Test compound preparation and addition to neurospheroids

All test compounds were of analytical standard or certified reference material purity (≥96–99%) and were obtained from Sigma-Aldrich (St. Louis, MO), Tocris Bioscience (Abingdon,UK), or Cayman Chemical (Ann Arbor, MI). Stock solutions were prepared in Milli-Q water (ddH_2O) (Millipore, Burlington, MA) or Dimethylsulfoxide (DMSO) solvent and kept frozen. Prior to obtaining the baseline recording, a 96-well glass-lined test compound addition plate (ThermoFisher #60180-P330) was prepared by dilution of serially diluted DMSO stock solutions into the phenol-red free test media. Six concentrations at half-log concentration decrements were prepared. Vehicles (0.1% DMSO or 3% ddH_2O) for time matched controls were also prepared. Prior to drug addition to the microplate, a 10 min baseline (BL) recording of Ca^{2+} spiking activity was obtained. Drugs were then added from the 96-well compound plate to the 384-well test plate via a 6× dilution (10 μl of 6× Test Concentration added to 50 μl well volume) with each test concentration applied to 4 neurospheroids (N = 4 wells) of a 384-well plate. The test plate was returned to the incubator and read at the following timepoints after test compound addition: 0 min (FLIPR only), 30 min, 60 min, 120 min, and where time would allow, 240 min.

2.2.3. Normalization of peak counts and peak amplitude

Averaged baseline-normalized peak count and peak amplitude values at each test concentration were normalized to baseline-normalized and averaged vehicle well values at the matched time point on that particular plate. This would compensate for any time-dependent drift of parameters from the original baseline reading at time $T = 0$ during the 2 h duration assay (when possible a 4 h read was also performed).

2.3. Mouse brain tissue isolation and cell dissociation

Experiments were conducted on C57BL/6J mice (Charles River Labs) according to the European Communities Council directive (86/609/EEC of 24 November 1986) and complied with the Directive 2010/63/EU of the European parliament and the related French transposition texts. The experiments were also approved by the local "Comité d'Ethique pour la Protection des Animaux de Laboratoire" (Animal Care and Use Committee) and are deemed compliant with the Sanofi Policy on the protection of animals. Neonatal brains (0–1 day old) of C57BL/6J mice were harvested and subjected to enzymatic dissociation: tissues were washed with neurobasal medium (2–8 °C) and resuspended in 6 ml Neurobasal, then incubated with 300 μl of trypsin (10×) and 150 μl of DNase (400 KU/ml). After 2–5 min of incubation at 37 °C, tissues received 2 washes with Neurobasal and 1% Bovine calf serum (37 °C). Mechanical dissociation followed, using 3 ml addition of NBC + 1% BCS (37 °C) then 10 gentle up and down aspirations with P1000 for dissociation. After 3–5 min the supernatant containing dissociated cells was harvested and filtered through a 40 μm filter.

2.3.1. Mouse dissociated cortical cell plating and maintenance

After 8 min centrifugation of the harvested cells at 1000 rpm, the supernatant was removed and cells resuspended with Neurobasal medium with N2 and B27 + 1% BCS (37 °C) and cells counted. Cells were plated at a density of 80,000 cells/well in Greiner polylysine coated 96 well black/clear bottom microplates. After a 30 s centrifugation at 1000 rpm the plates were placed into an incubator at 37 °C, 5% CO_2 and 80% humidity. The culture medium was renewed 24 h after cell plating and then every 2–3 days with visual inspection of cells under microscope. Mouse cortical composition may be roughly 25% astrocytes and 75% neuronal cells, of which 20% are GABAergic and 80% are glutamatergic.

2.3.2. Ca^{2+} sensitive dye loading of mature network of mouse cortical neurons

After network formation of 16 days in vitro (±1 day), the medium was removed and cells incubated with a dye loading medium (100 μl/well) consisting of HBSS saline solution containing 2 mM of Mg^{2+}, Cal520-AM probe (ATTBioquest®, 1/200th dilution), Powerload (ThermoFisher, 1/100th dilution), a non-ionic surfactant to help disperse the acetoxymethyl probe, and Probenicid (Thermofisher®, 1/100th dilution) to retard cellular extrusion of the probe. After 1 h loading at 37 °C in 5% CO_2 plates were washed 3 times with HBSS medium containing 0.1 mM of Mg^{2+}. The low concentration of Mg^{2+} facilitates Ca^{2+} entry into neurons through NMDA receptors. Plates were incubated 10 min at 37 °C in 5% CO_2 between each wash.

2.3.3. Compound preparation and addition in Hamamatsu FDSS plate reader

Meanwhile, a 96-well glass-lined addition plate (="product plate") containing test compounds in HBSS containing 0.1 mM Mg^{2+} was prepared with a range of concentrations for each, vehicle and positive controls 4-Aminopyridine (30 μM) and MK-801 (30 μM). For fluorescence detection, the μCell FDSS instrument (Hamamatsu®) was used, a kinetic plate reader with an integrated dispensing head and imaging-based detector. The protocol was designed to first read 7.5 min of activity prior to addition of compound. Then, the automated instrument dispensed simultaneously the compound of interest from "product plate" to "cellular plate" in each well (20 μl/well) while continuing to read the Ca^{2+} fluorescence in each well for 7.5 additional min. During this 15-min recording, two parameters are measured in each well: oscillation frequencies and amplitudes (before and after compound injection). Data output for frequency and amplitude are obtained with Waveanalysis® software from Hamamatsu© and are given in Relative Fluorescence Unit (RFU) and used for data analysis. Final concentration of DMSO was 0.1% during compound testing. Parameters were normalized to preinjection values, then to vehicle mean, and then averaged and are reported as Mean ± SE from 6 or 12 wells at each test concentration.

2.4. 2D hiPSC derived neuron culture

Fujifilm Cellular Dynamics, Inc. (FCDI) iCell® GlutaNeurons (donor 01279, # R1034) and iCell Astrocytes (donor 01434, # R1092) were plated and grown according to manufacturer instructions in a supplemented BrainPhys Neuronal Medium (STEMCELL Technologies #05790). Prior to cell plating, microplates (Greiner 96- or 384-well) were prepared by coating with 0.07% Polyethylenimine (PEI) in Hank's Balanced Salt Solution (HBSS) for 1 h at room temperature. After 3 washes with HBSS, Matrigel (0.028 mg/ml) diluted into complete BrainPhys medium was added to the plates and incubated for 1 h at 37 °C. After removal of Matrigel solution, iCell GlutaNeurons and iCell Astrocytes were plated in a 4:1 ratio at 80,000 cells per well in 96-well plates (100 μl each well), and 25,000 cells per well in 384-well plates (75 μl each well). GlutaNeurons are a mixture of about 70% glutamatergic and 30% GABAergic neurons. Plates were incubated at 37 °C, 5% CO2, and the media was changed every 2 days.

2.4.1. Calcium imaging of 2D hiPSC derived neuron networks

At neuronal maturity of 23 days in vitro (±1 day), the media was removed, and cells incubated with dye loading medium (75 μl/well) composed of BrainPhys medium containing Cal520-AM probe (ATTBioquest®, 1/200th dilution), Powerload (#P10020, ThermoFisher, 1/100th dilution), a non-ionic surfactant to help disperse the acetoxymethyl probe, and Probenicid (#P36400, Thermofisher®, 1/100th dilution) to retard cellular extrusion of the probe. Cells were incubated with this loading medium for 1 h at 37 °C, in 5% CO2. Plates were then washed 3 times with Brainphys medium without phenol red and without protein. Plates were incubated 10 min at 37 °C, in 5% CO2 between each wash. Meanwhile, a "product plate" containing compounds of interest diluted in BrainPhys without phenol red and 0.1% DMSO (Sigma-Aldrich ®) was prepared with a range of concentrations for each compound of interest and vehicle (corresponding to BrainPhys without phenol red with 0.1% DMSO), as well as positive reference compounds 4-AP (30 μM) and MK-801 (10 μM).

For fluorescence detection the FDSS μCell instrument (Hamamatsu®) was used (see above for Mouse Cortical Neurons) with an integrated dispensing head (either 96- or 384-well). The automated instrument dispenses simultaneously the compound of interest from "product plate" to "cellular plate" in each well (15 μl/well) and detects simultaneously fluorescence in each well. Ca^{2+} flux oscillation variations were captured continuously for 20 min. Prior to the injection starting at 10 min after the beginning of recording, a 10-min baseline was recorded. Two parameters were measured in each well: Ca^{2+} oscillation frequencies and amplitudes (before and after compound injection). Data output for frequency and amplitude were obtained with Waveanalysis® software from Hamamatsu© and are given in Relative Fluorescence Unit (RFU) and used for data analysis. Well parameters were normalized to preinjection values, then to vehicle mean, and then averaged and are reported as Mean ± SE from 8 wells at each test concentration.

3. Results

Figs. 1A,B show the highly reproducible sizes of the tested neurospheroids imaged using light microscopy. The average diameter of neurospheroids in six 384-well test plates ranged from 0.59 to 0.69 mm with a coefficient of size variation of only 1.3%–2.3% across the plates. This highly reproducible neurospheroid size underlies the highly reproducible Ca^{2+} spiking signals across the plate wells, as shown in Fig. 1C from the same neurospheroids as shown in Fig. 1A. Plotted are the spontaneous Ca^{2+} oscillations of all 384 neurospheroids over a 10 min baseline recording. The Ca^{2+} traces shown are from plate FDSS-3, with an average number of peak counts observed over the 10-min recording of 53 peaks (5.3 peaks/min) with a standard deviation of

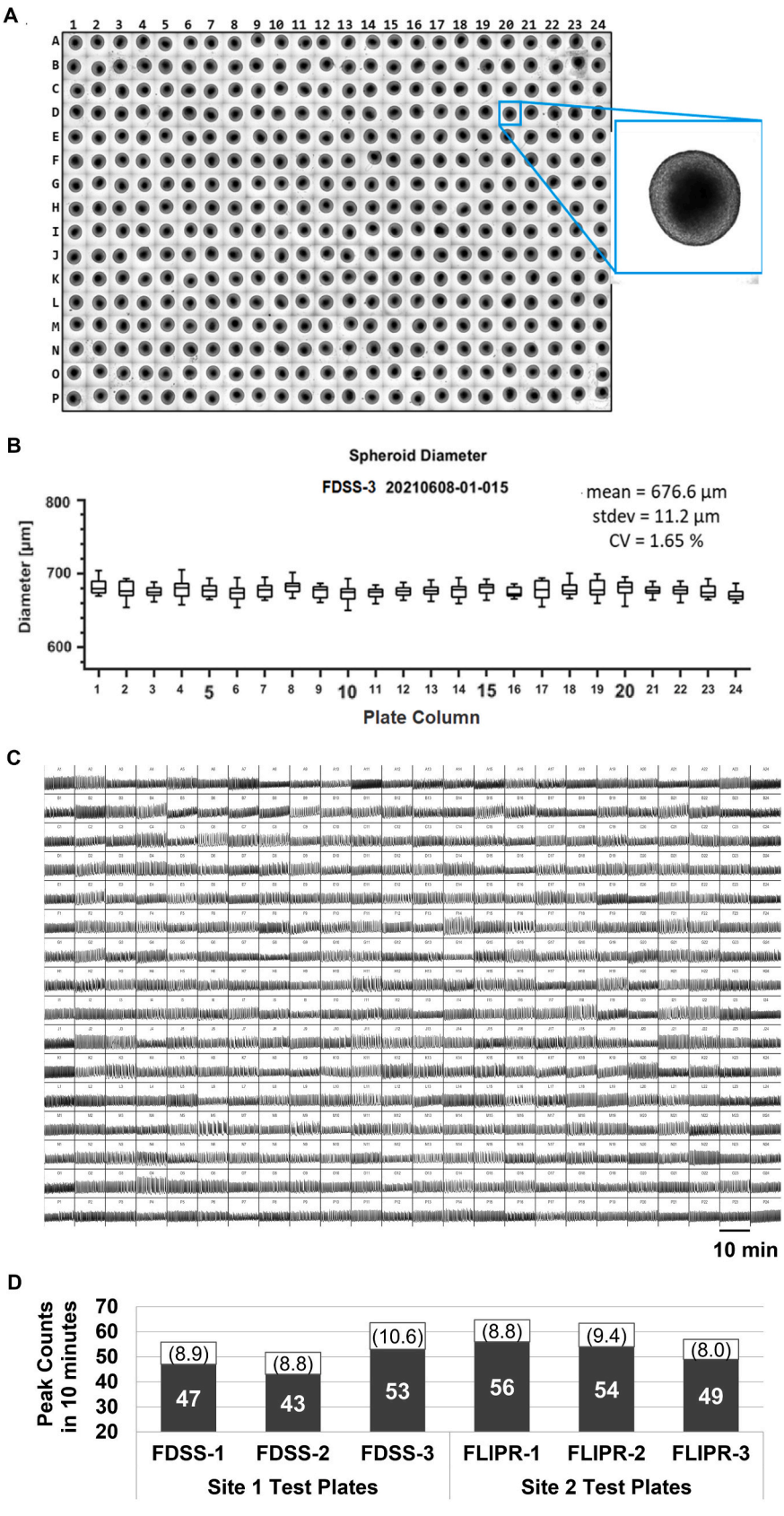

Fig. 1. Neurospheroid morphology and calcium spiking in 384-well imaging plates.

(A) Light microscopic images of the arrayed neurospheroids prior to shipment (image provided by vendor). The inset shows the near spherical shape of a magnified neurospheroid. (B) Box plots of neurospheroid sizes for each of the 24 columns (N = 16 neurospheroids/column) of the plate in A. The average size of plated neurospheroids was 677 µm (± 11.2µm, SD) yielding a coefficient of size variation of 1.65%. (Plot provided by the vendor).

(C) Baseline Ca^{2+} transients imaged from a 384-well plate after loading with Calcium6 dye. Ten minutes of recording time are shown for each of the 384 wells arranged according to position in the 384-well plate. The mean spiking rate averaged from 384 neurospheroids in the plate over the 10-min recording period was 5.3 +/− 1.06 spikes per minute (mean +/− SD, Plate FDSS-3). (D) Each column indicates the mean (SD) baseline peak counts over 10 minutes of a 384-well neurospheroid plate used in the Ca^{2+} imaging test platform located at each test site.

10.6 peaks (1.06 peaks/min) (N = 384 neurospheroids) for this plate. Fig. 1D graphs the peak count statistics of the six plates used in this study. Three plates were tested at each site and baseline peak counts were comparable across the sites. The coefficient of variation of peak counts within a plate ranged from 16% - 21% and attests to the reproducibility of the biology underlying the neurospheroid generation by the supplier.

Fig. 2A illustrates the Ca^{2+} oscillation responses of 12 neurospheroids each to vehicles, positive control 4-Aminopyridine (30 μM 4-AP), a non-selective voltage-gated potassium channel blocker, and inhibitory control Muscimol (10 μM), a selective $GABA_A$ channel agonist, 2 h after addition to the 384-well plate. For comparison, typical responses of the hiPSC derived 2D networks of iCell GlutaNeurons and Astrocytes are shown in Fig. 2B to positive controls 4-AP (30 μM) and MK-801 (30 μM), a non-selective NMDA receptor blocker. Note the marked increase in Ca^{2+} peak frequency of both 2D and 3D hiPSC networks to the voltage-gated potassium channel blocker 4-AP over the 10-min recording durations. Similar increases in Ca^{2+} spiking activity in response to 4-AP and decrease or cessation of activity by MK-801 were observed in the 2D primary mouse cortical neuron preparation that we investigated (not shown), and have been previously reported in the literature (Pacico & Mingorance-Le Meur, 2014; Roussignol et al., 2017). Larger effects by 4-AP on peak frequency were observed in the 2D hiPSC networks than either the 2D mouse cortical or 3D neurospheroid networks (Fig. 2C). Effects on peak amplitude by 4-AP were more divergent between the models. Considering that iCell GlutaNeurons are a population of primarily glutamatergic neurons (>70% according to the manufacturer), it is possible that differences in cell subtype composition in the three models could determine the observed differences in Ca^{2+} spiking activity in response to these compounds.

Fig. 3 illustrates the effect of the native neurotransmitter GABA on Ca^{2+} spiking of the neurospheroids. The neurospheroids are composed of approximately 10% GABAergic neurons according to the vendor. Shown are the results from the two test sites, aligned according to concentration for comparison of effects in the two assay platforms. Each of six half-log steps in concentration up to 500 μM were tested in four neurospheroids, as shown in the 2 × 2 grid under each of the indicated concentrations. In both the FLIPR and FDSS plate reader platforms 50 μM was the GABA threshold concentration above which no more Ca^{2+} spiking could be observed, as higher concentrations completely abolished the spontaneous Ca^{2+} spiking of the neurospheroids. The similarity of Ca^{2+} peak frequency and amplitude responses of the neurospheroids across sites and assay platforms attested to the reproducibility of neurospheroid composition and biology. This is further supported by the congruence of both frequency and amplitude responses measured at the two test sites for all NeuroDeRisk test compounds as shown in Fig. 5. GABA was not tested in either 2D model.

Fig. 4A illustrates the effect on neurospheroid Ca^{2+} activity of Kainic acid, a non-specific glutamate and AMPA receptor agonist, used widely to induce seizures in animal models of temporal lobe epilepsy (Levesque & Avoli, 2013). The results obtained at two separate sites on two separate platforms using identical compound stocks illustrates the reproducibility of the observed effect of decreased peak amplitudes of Ca^{2+} activities by this ictogenic compound in the neurospheroid model. Fig. 4B illustrates similar concentration-dependent decrease in peak amplitude in the hiPSC neuronal 2D. The mouse 2D cortical network initially also displayed a concentration-dependent decrease in amplitude, however at higher Kainic acid concentrations (10 μM and 30 μM) a reversal of the amplitude effect and large gain in amplitude was apparent. Excitation resulting from stimulation of the ionotropic glutamate receptors is known to cause the increase in intracellular calcium and trigger calcium-dependent pathways that lead to potential

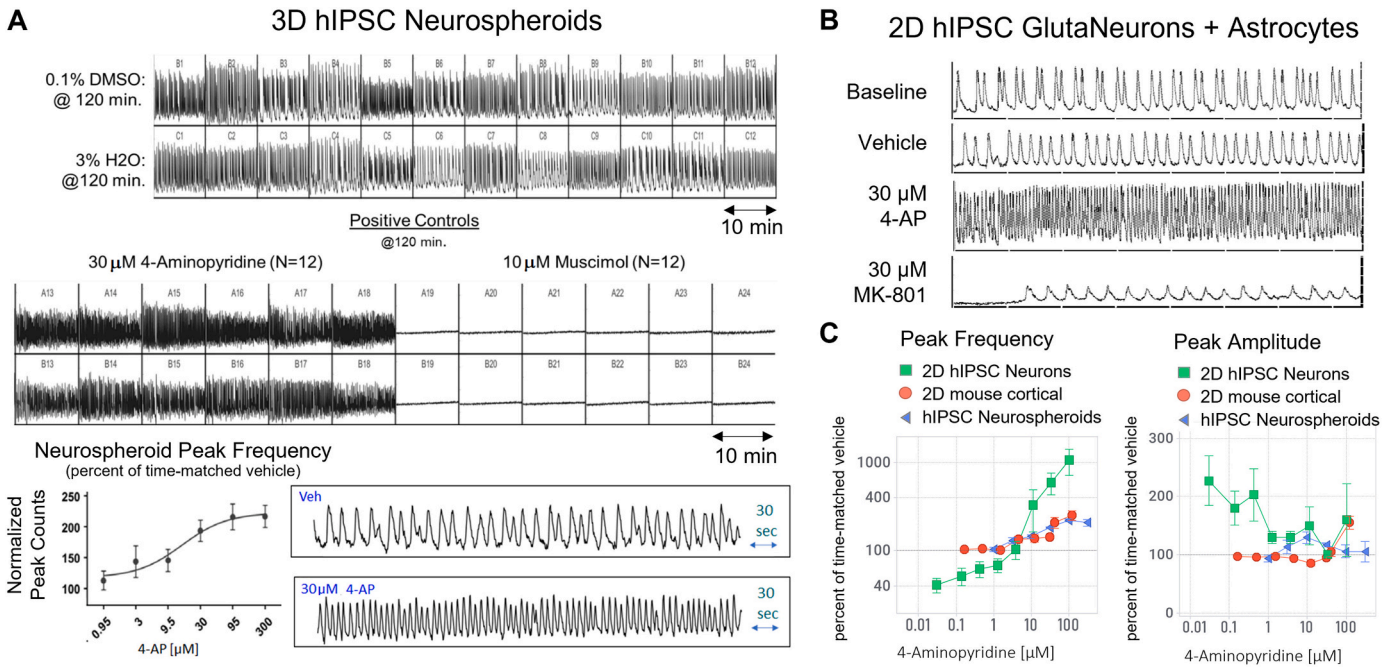

Fig. 2. Ca^{2+} spiking activity in response to positive controls in hiPSC neurospheroids and 2D networks.
(A) Ca^{2+} spiking signals from Vehicle (0.1% DMSO and Water (H2O)) wells and Positive Controls (30 μM 4-Aminopyridine and 10 μM Muscimol) wells 2 h after application to the wells over a 10-min recording period. (N = 12 neurospheroids at each condition). 4-Aminopyridine (4-AP, 30 μM), a voltage-gated potassium channel blocker, is excitatory, whereas the GABA agonist Muscimol (10 μM) is inhibitory and causes complete cessation of the spiking. Concentration-response of normalized Peak Frequency over 10 min, reported as percent of time-matched vehicle values. 4-AP was tested at concentrations of 0.95 μM to 300 μM (N = 4, each concentration). Error bars are standard error of the mean. (Plate FDSS-1) (B) Representative Ca^{2+} responses of 2D hiPSC iCell GlutaNeuron and iCell Astrocyte networks. Traces show 15 min of continuous activity in the presence of the indicated positive control compound concentrations. MK-801 (10 μM) is a non-selective NMDA receptor antagonist. (C) Comparison of the effects on Ca^{2+} spiking activity of 4-AP on the 2D and 3D neuronal network models as assayed using plate-based Ca^{2+} fluorescence platforms (mean ± SE, for N see Methods). Peak Frequency and Amplitude are normalized to vehicle. For 2D neuronal models, the commencement of the Ca^{2+} fluorescence recording followed immediately upon the application of the compound to the test plate.

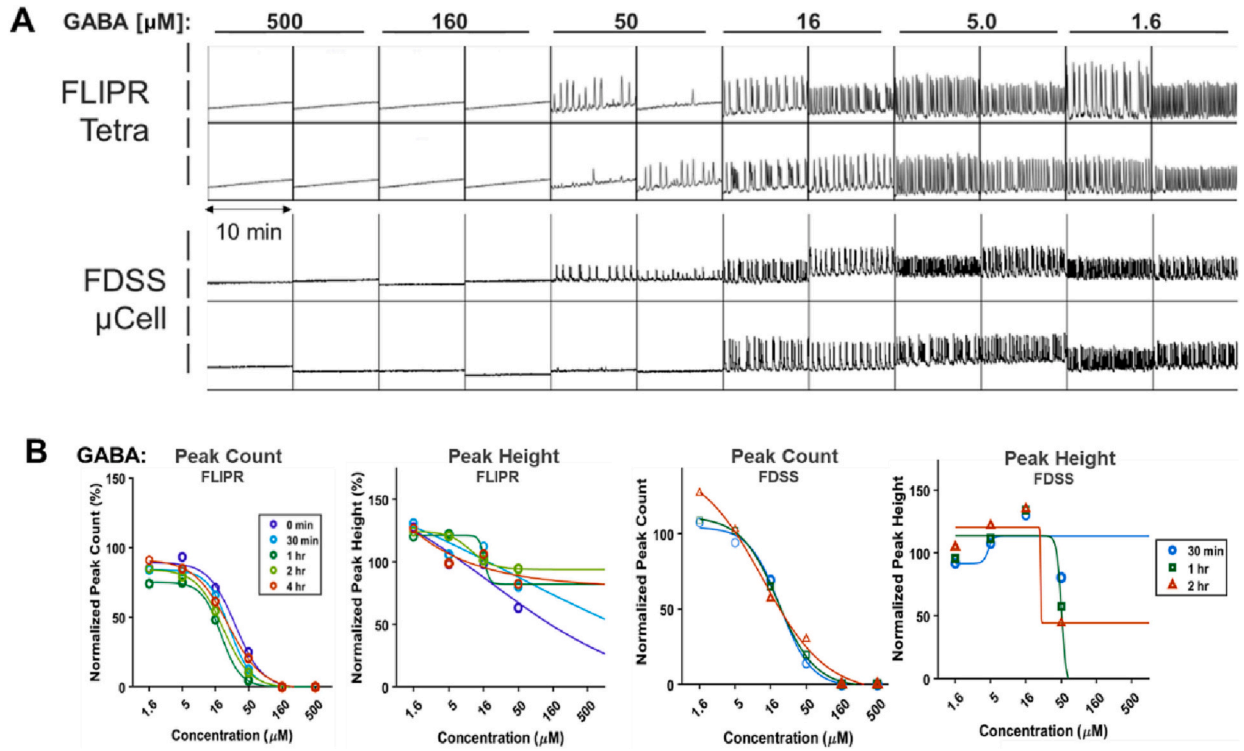

Fig. 3. Effect of GABA on Neurospheroid Ca^{2+} activity in two plate readers tested at two different sites. (A) GABA concentrations were applied at half-log concentrations up to 500 μM. Each concentration was applied to four adjacent wells (2 × 2) and incubated for two hours before reading Ca^{2+} activity in the FLIPR or FDSS platform. Cessation of spontaneous spiking activity was observed at concentrations >50 μM in both platforms. (B) Concentration-response curves of Peak Counts and Peak Amplitudes for GABA as measured in the two test platforms at the two test sites (FLIPR, left panels; FDSS, right panels). Different colors correspond to the indicated time delays before commencement of the Ca^{2+} fluorescence recording following the application of the compound to the test plates. Normalized peak counts and peak amplitudes over the 10-min recording duration were averaged after normalizing to the baseline (Pre-addition) value for each well as well as to time-matched vehicle controls. The threshold concentration at which slowing of spiking activity could be clearly observed was 16 μM GABA in both test platforms.

exaggerated physiology or functional toxicity. In this context, it is interesting to note that while the hiPSC 2D network showed increases in frequency with high test concentration of Kainic acid (30 μM and 100 μM) the mouse cortical 2D network responded with strong decreases in frequency to this highly ictogenic tool compound.

Given the similarity in peak frequency responses to the potassium channel blocker 4-AP between the different models (Fig. 2), it may be attractive to conclude that an increase in activity in Ca^{2+} spiking frequency would be a tell-tale phenotype of an ictogenic compound. However, the variability in frequency and amplitude responses to Kainic acid as observed between the different models (Fig. 4) suggests that the assignment of ictogenic risk to a test compound based on directional responses in either Ca^{2+} peak frequency, peak amplitude, or both, may not be straightforward. To explore a potential functional signature of an ictogenic compound, we tabulated the directional effects by each test compound on the frequency and amplitude parameter changes in the different models in Table 2.

Table 2 lists the NeuroDeRisk compound set grouped according to the assigned categories of tool compounds experimentally known to cause seizures (Tool) and clinical compounds with documented seizurogenic risk based on pharmacovigilance databases (FAERS Positive or Negative) (see Methods). To simplify, directional assessment responses were assigned either +1 for an increase, −1 for a decrease, and 0 for lack of significant change to either frequency or amplitude of the Ca^{2+} oscillations. Each assay parameter directional effect is compared to the other two assay results and, if they match, are highlighted in light green in the Table 2. The best match (20/26, or 77%) is between the Frequency responses of the 3D hiPSC neurospheroid assay and the mouse cortical neuron 2D network (CTX) assay. The poorest matches were between the hiPSC models, where 2D hiPSC neuronal networks vs. 3D hiPSC neurospheroid matched only 38% for Frequency and 50% for Amplitude.

Given the higher overlap between neurospheroid and mouse cortical neuron responses, we plotted their concentration responses for Tool compounds, FAERS positive and FAERS negative compounds. Tool compound effects on the spontaneous Ca^{2+} spiking activity are presented in Fig. 6 in alphabetical order. Notable is that all tool compounds tested have effects on frequency or amplitude except Strychnine (only tested in neurospheroids). Pilocarpine, a muscarinic cholinergic agonist, decreased frequency slightly in both models, and with time showed an apparent increase in spike amplitude in the neurospheroid model. Bicuculline and Picrotoxin, both GABA antagonists, produced similar effects in the mouse cortical model, characterized by marked decreases in spiking frequency accompanied by large increases in amplitude. In contrast Bicuculline had no clear concentration dependent effects in neurospheroids. Donepezil, an acetylcholinesterase inhibitor, and Kainic acid also produced this pattern in the mouse cortical model, but to a lesser extent. Chlorpromazine reduced peak counts at a threshold concentration of 10–30 μM. Delta-opioid receptor agonist SNC-80 (tested only in neurospheroids) reduced both frequency and amplitude in a time-dependent manner. Tool compound Pentylenetetrazole (a GABA antagonist) was tested as high as 6 mM yet had only a limited effect on frequency and decreased amplitude only at the highest concentrations in neurospheroids.

Remarkably, 7 out of 9 tool compounds tested in the neurospheroid and mouse cortical models matched directional changes in frequency (shaded cells in Table 2), whereas only 3 out of 9 compounds matched directional changes in amplitude. Concordance in directional effects on frequency were also observed with the FAERS positive set of compounds (Fig. 7). These clinical compounds have been found to have reports of

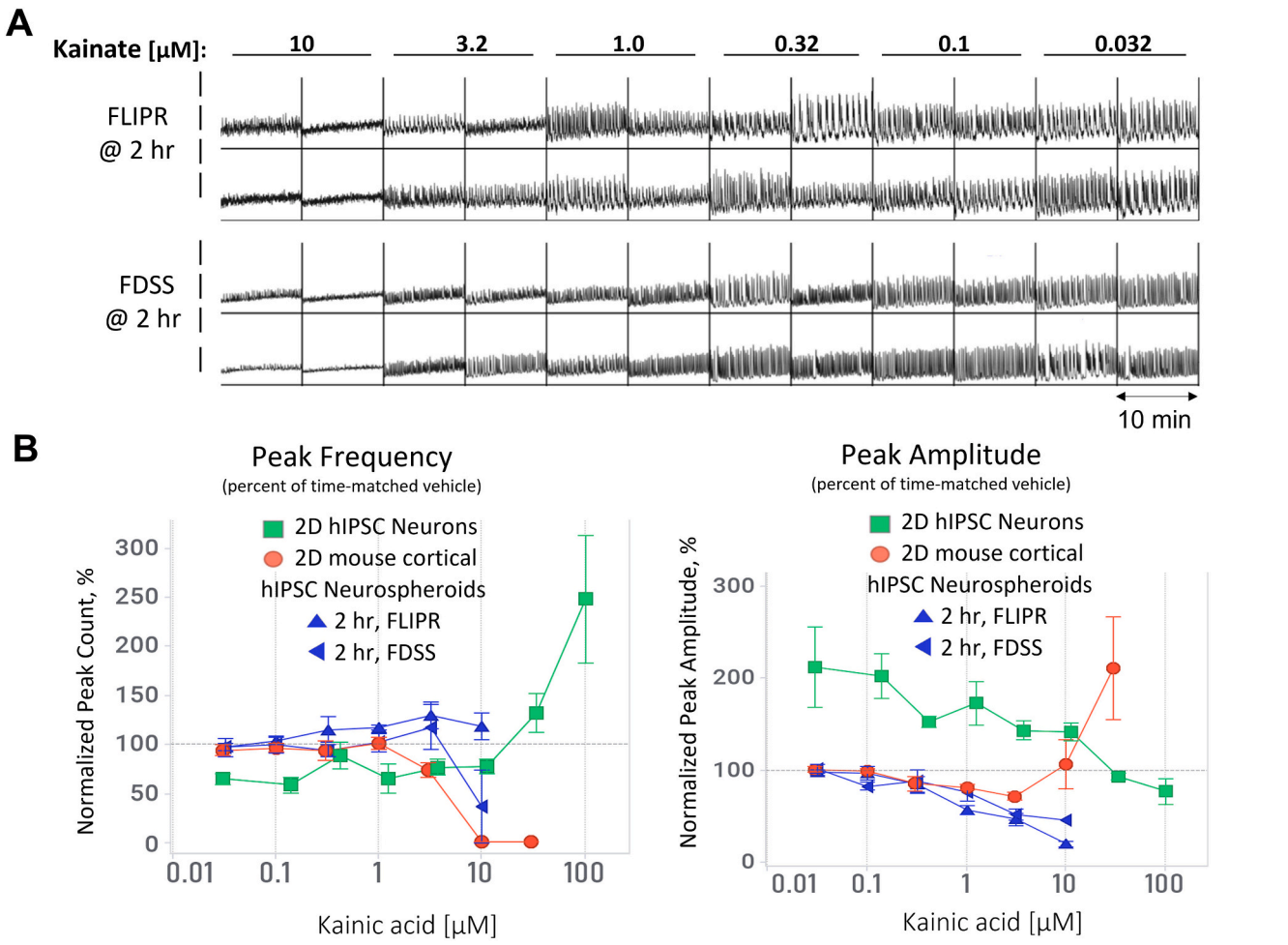

Fig. 4. Effect of Kainic acid on Ca^{2+} activity of different network models. (A) Kainic acid concentrations were applied to neurospheroids at half-log concentrations up to 10 μM and the signal recorded for 10 min. Each concentration was applied to four adjacent spheroids (2 × 2) and incubated for 2 h before reading Ca^{2+} activity in the FDSS platform (site 1) or the FLIPR platform (site 2). (B) Comparison of frequency and amplitude responses to Kainic acid in the different network models. For the 2D hiPSC neuron model (filled green squares, ■) and the 2D mouse cortical model (filled red circles, ●), commencement of recording of Ca^{2+} spiking started immediately upon addition of compound to plate. For the neurospheroid responses shown in (A), recording commenced 2 h after compound addition and concentration-responses for both the FLIPR (▲) and FDSS (◀) platforms are shown (filled triangles, blue). (For interpretation of the references to colour in this figure legend, the reader is referred to the web version of this article.)

seizures as adverse events according to the FDA database of adverse event reporting. Out of 8 compounds tested in both models, 7 compounds showed matching directional effects on frequency with concentration-responses largely overlapping. The main effect of these compounds was to decrease the spontaneous Ca^{2+} spiking activity of the networks. Notably, Theophylline, an adenosine receptor antagonist, was the exception as it increased frequency in both models in a graded manner. The effects of the FAERS positive compounds on Ca^{2+} spiking amplitude reveal that most compounds also decrease amplitude in the models. Furthermore, the directional effects on amplitude are largely shared between the models, except for Mirtazapine, an antidepressant with complex antagonistic activity at histamine, alpha-adrenergic, and serotonergic receptors, which led to amplitude increases in the mouse model and decreases in the neurospheroid. As with frequency, the majority of compounds matched directionality of amplitude changes in the mouse cortical and neurospheroid models. The close match between the Ca^{2+} responses of the native primary cortical network and the neurospheroid support the cortical characterization of the hIPSC model.

Fig. 8 illustrates the more muted responses of the mouse model to FAERS negative compounds. These are compounds that have not been associated with seizurogenic adverse events based on pharmacovigilance reporting. Of the 9 compounds tested in the mouse model, only Azelastine completely stopped Ca^{2+} spiking, compared to 5 cases of complete spiking cessation observed with FAERS positive compounds (Fig. 7). Reduced effects were observed for amplitude, as well, and the mouse cortical model reported smaller effects on amplitude compared to the neurospheroids. Roflumilast, a PDE4 inhibitor, decreased amplitude and increased frequency in the neurospheroids at all concentrations, but lacked any effect in the mouse model. Minoxidil, an IK_{ATP} inhibitor, and the vitamin Niacin were the only FAERS negative compounds where minimal effects on both frequency and amplitude were observed in the neurospheroid model.

Considerable variability in responses were observed across the compound categories and across models for a given compound (Table 2). After having compared the mouse cortical and neurospheroid responses of FAERS positive and FAERS negative compounds (Figs. 7 and 8), the most common effects to be attributed to FAERS positive compounds were the reduction of the rate of Ca^{2+} spiking as well as the amplitude of the Ca^{2+} spikes. Interestingly, these combined effects were not shared by the hiPSC 2D network model (Table 2 and Fig. 9). Rather, in the hiPSC 2D model, the effects on frequency were more variable in their concentration responses and therefore more difficult to interpret. Both FAERS positive and negative compounds tended to increase frequency and to decrease amplitude in the hiPSC 2D network model and no clear

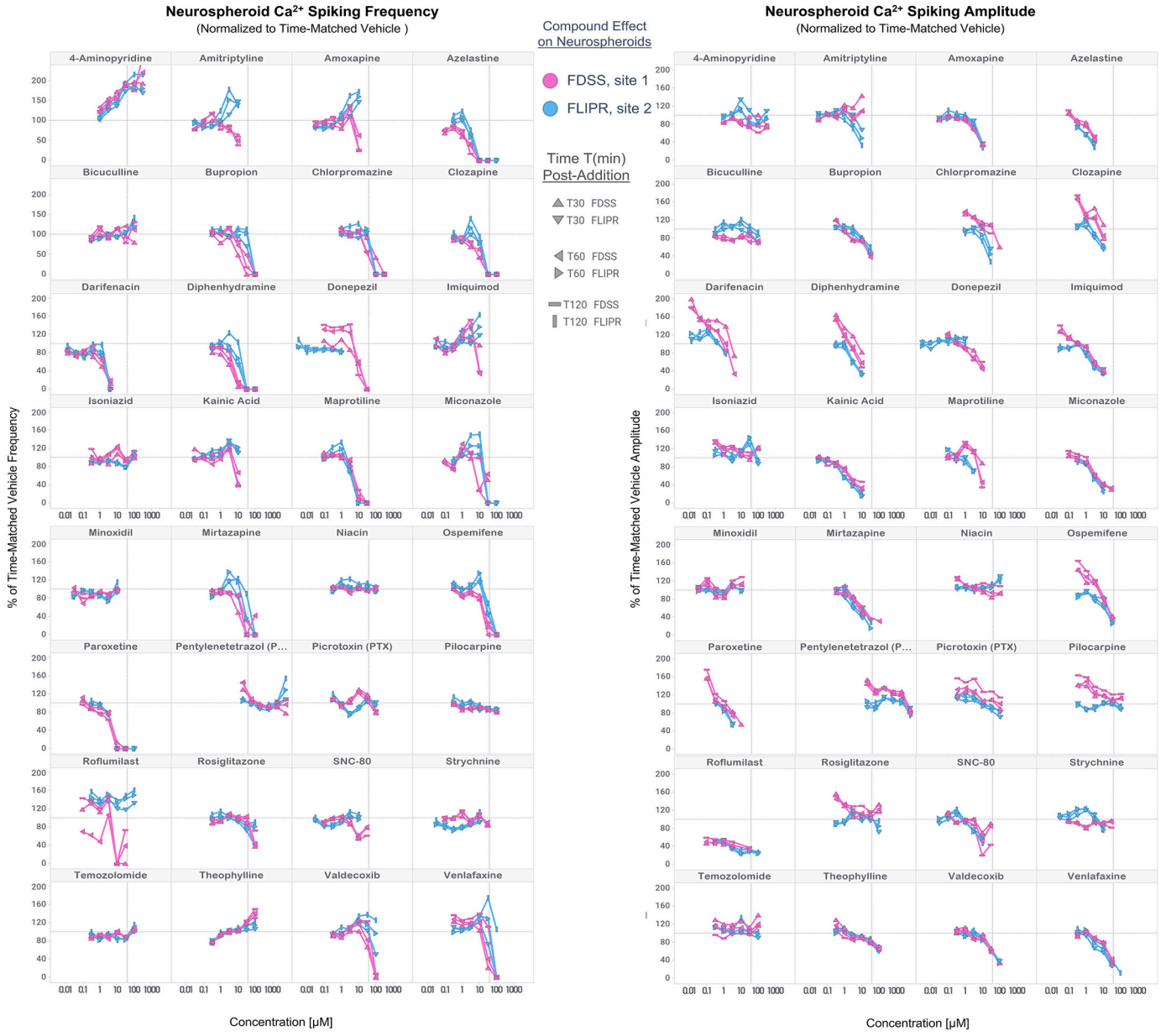

Fig. 5. Comparison of responses to NeuroDeRisk compounds of hiPSC neurospheroids in the FDSS and FLIPR Ca^{2+} imaging platforms.
Plots of concentration-response curves of Ca^{2+} oscillation frequency (left panel) and amplitude (right panel) to the NeuroDeRisk compound set. Neurospheroid responses were assayed using identical protocols and compound stock solutions at 30 min, 1 h, and 2 h following drug application at two sites using either FLIPR platform (light blue (30▼,60▶,120 ▌min)) or FDSS platform (lavender (30▲,60◀, 120 ═ min)) (average, n = 4 wells per concentration).

distinction could be made between categories based on this parameter.

Since parameter changes in the different models were complex, insight into potential patterns that may be predictive of ictogenicity were sought with contingency table analysis. Table 3 presents the predictivity of the different network models for the NeuroDeRisk FAERS positive and negative compounds using different criteria for what type of changes to frequency or amplitude constitute a positive for seizurogenic risk. The table is meant for comparative purposes only as it does not take into consideration many criteria that would factor into the adequacy of such a predictive exercise. For example, a key component of such an evaluation would be to understand the brain exposure to each compound in the clinic when the adverse event occurred, such that clinical free concentrations could be directly compared to test concentrations and their effects in the network models, and thresholds for ictogenicity set accordingly. Nevertheless, it is instructive to see how the different network models were able to predict risk of seizurogenicity based on a straightforward interpretation of parameter changes over the tested concentration ranges.

Case 1 in Table 3 assesses how the different models score when any directional change to either parameter constitutes a risk. In this most conservative evaluation, the mouse cortical model would detect 7 of 8 tested FAERS positive compounds (88% sensitivity) but would misidentify FAERS negatives as positives in 7 out of 9 cases (22% specificity). The Youden Index (YI), a measure of the overall predictive utility of the assay (YI=Sensitivity+Specificity−1, with YI $\leq$ 0 having no utility, and YI = 1 having perfect predictivity) was only 0.1 using this criterion (Youden, 1950). Maximizing the Youden Index weights sensitivity and specificity of a diagnostic test equally and seeks to maximize both, i.e. by minimizing both false negatives and false positives. The hiPSC 2D network and 3D neurospheroid models also scored poorly under Case 1 criteria (Youden Indexes of YI $\leq$ 0.0 and 0.03, respectively) illustrating that simply using changes to a Ca^{2+} oscillation parameter to

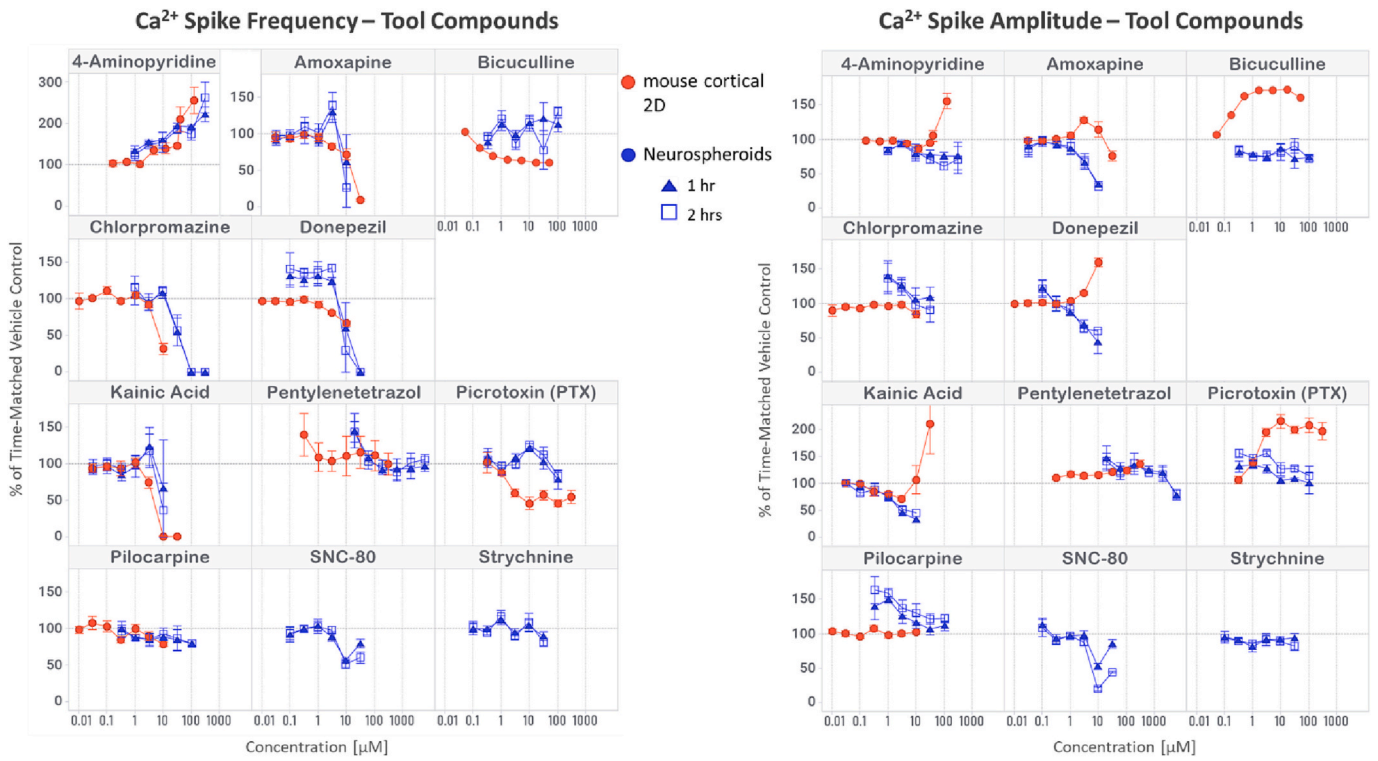

Fig. 6. Comparison of responses to seizurogenic tool compounds of hiPSC neurospheroids and mouse cortical neurons.
Plots of concentration-response curves of Ca^{2+} oscillation frequency (left panel) and amplitude (right panel) to seizurogenic tool compounds (Mean ± SE). Neurospheroid responses at 1 h (▲) and 2 h (□) after compound addition are shown in blue (n = 4 wells). Mouse cortical neuron 2D network responses are shown in red (●) (n ≥ 6 wells).

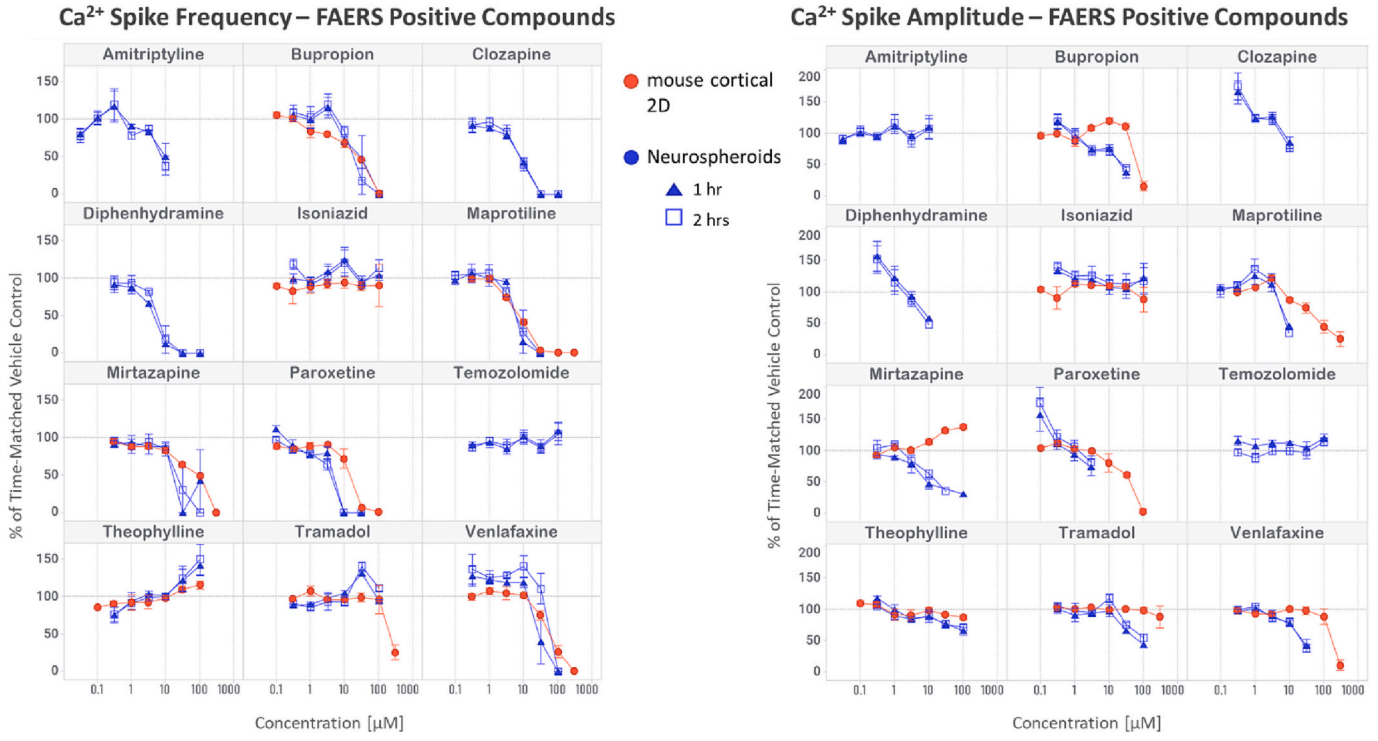

Fig. 7. Comparison of responses to FAERS seizurogenic positive compounds of hiPSC neurospheroids and mouse cortical neurons.
Plots of concentration-response curves of Ca^{2+} oscillation frequency (left panel) and amplitude (right panel) to drugs which are associated with seizures (Mean ± SE). Neurospheroid responses at 1 h (▲) and 2 h (□) after compound addition are shown in blue (n = 4 wells). Mouse cortical neuron 2D network responses are shown in red (filled circles, ●) (n ≥ 6 wells).

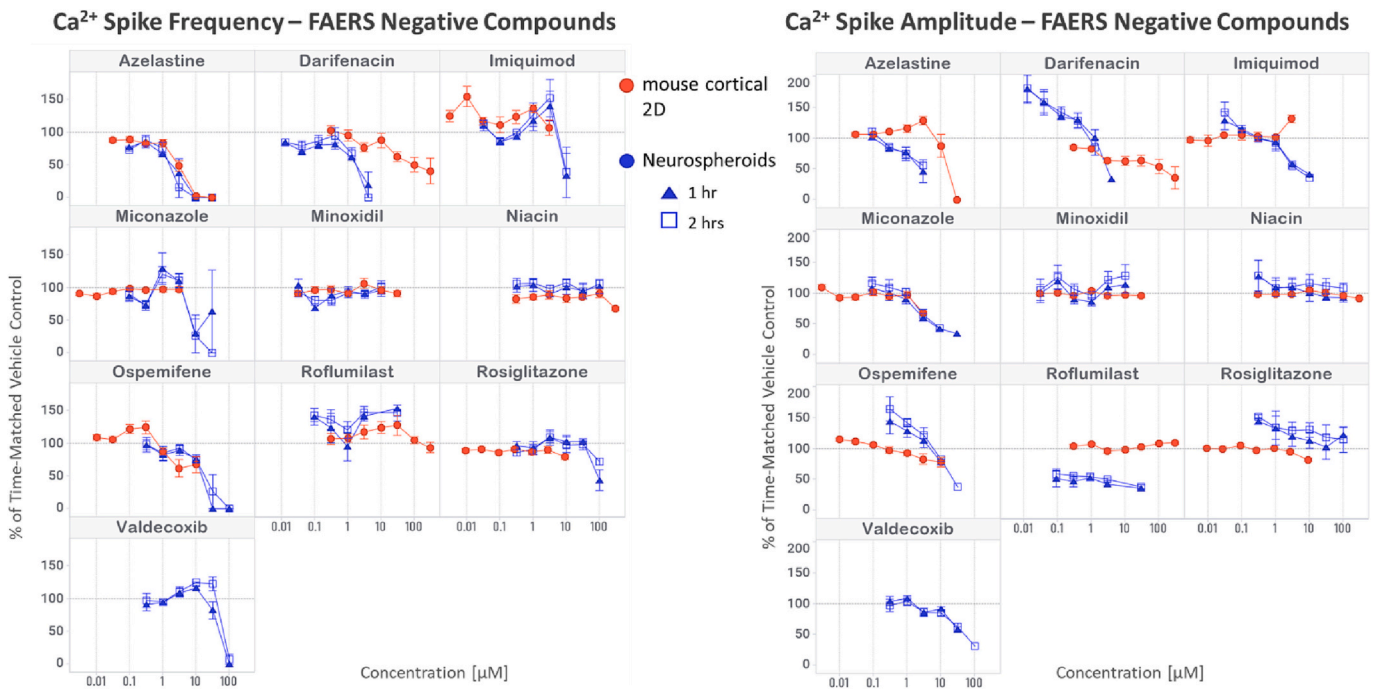

Fig. 8. Comparison of responses to FAERS negative compounds of hiPSC neurospheroids and mouse cortical neurons.
Plots of concentration-response curves of Ca^{2+} oscillation frequency (left panel) and amplitude (right panel) to drugs which are not associated with seizures (Mean ± SE). Neurospheroid responses at 1 h (▲) and 2 h (□) after compound addition are shown in blue (n = 4 wells). Mouse cortical neuron 2D network responses are shown in red (filled circles,●) (n ≥ 6 wells).

assign risk yields poor diagnostic value.

If the assignment of risk is more limited, such as ascribing changes to only the frequency parameter as an indicator of risk (Case 2, Table 3), the contingency analysis yields improved predictivity outcomes in the 2D mouse network model (YI = 0.21), however, both hiPSC derived models still suffer high false positives. If ictogenicity is limited to compounds causing decreases in frequency (Case 3), the predictivity of the neurospheroid model improves (YI = 0.27) due to increased specificity of 60%. The predictivity of the neurospheroid models was further improved by requiring decreases in both frequency and amplitude (Case 4). These criteria further reduced the false positive rate to only 3 out of 10 compounds, yielding a specificity of 70% at the expense of a slightly increased false negative rate from 4 out of 12 to 5 out of 12 compounds (58% sensitivity). Combined decreases in both frequency and amplitude as the ictogenic criteria yielded the maximal Youden index (YI = 0.28) for the neurospheroid model and a near maximal YI for the mouse cortical model (YI = 0.31), as well.

Interestingly, decreases in amplitude as a criterion by itself (Case 5, Table 3) yielded maximal Youden Index for both 2D models (YI = 0.32 for the mouse cortical model, and YI = 0.29 for the hiPSC neuronal model), while being of poor diagnostic value in the neurospheroid model due to a high false positive rate (specificity = 30%). Interestingly, increases in Ca^{2+} oscillation frequency in response to FAERS positive and negative compounds were observed in the 2D hiPSC neuronal model where this diagnostic criterion (Case 6, Table 3) yielded relatively good sensitivity (88%) but poor specificity (33%) (YI = 0.21). It is apparent from these types of analyses that using fixed criteria and thresholds for scoring of a diagnostic test always balances sensitivity with specificity, and that decision making will also involve the relative costs of false negatives (cost of developing an unsafe compound) and false positives (cost in opportunity to discontinue a potentially efficacious and safe compound) in deciding how to proceed following safety screening assays. The binary contingency analysis presented above should be seen as a starting point from which to understand the general responses of these networks to compounds with clinically demonstrated ictogenicity. Interpretation of Ca^{2+} oscillation parameters will need additional refinement to make distinctions between potentially desired pharmacological effects of a neuroactive compound and ictogenic side effects of compounds which may or may not be targeted to the brain.

4. Discussion

The finding that a decrease in Ca^{2+} oscillation frequency in cortical models is an important, though not fully predictive marker of adverse neural function based on contingency analysis (Cases 3 and 4, Table 3) has been borne out by other studies on neurospheroids. Three previous studies have studied large sets of compounds in the neurospheroid model. In the first (Sirenko et al., 2019) a study of 87 compounds that included pharmaceutical drugs, pesticides, flame retardants, and other chemicals revealed that the majority of neuroactive compounds caused decreases in the rate of Ca^{2+} spiking, and these effects were reproducible between successive repeats of the assay. In a second study of a large library of pharmacologically active compounds (1024), of the 77 compounds active on neurospheroid Ca^{2+} spiking only 9 compounds (12%) caused increases in the Ca^{2+} spiking rate, while the rest caused decreases in Peak Counts (88%) (Woodruff et al., 2020). In a third investigation of a large (687) set of clinical and tool compounds, cluster analysis of Ca^{2+} activity responses revealed that peak count decreases and peak amplitude changes were key determinants in the assignment of compounds into one of three main clusters (Boutin et al., 2022). Modelling genetic forms of clinical epilepsy in hiPSC derived neurons has also revealed phenotypes of reduced network or neuronal activity relative to wildtype controls (Costa et al., 2016; Dalgin et al., 2021; Marchetto et al., 2010; Sundberg et al., 2018). The slow global Ca^{2+} transient extends over many seconds and is an indicator of maintained synchronized activity throughout the network. It is therefore reasonable that any drug that interferes with synaptic transmission or neuronal excitability would tend to decrease maintenance of this activity. There remains the question of the role of the astrocytes in the network and to what extent their influence contributes to shaping of the Ca^{2+} response. Genetically

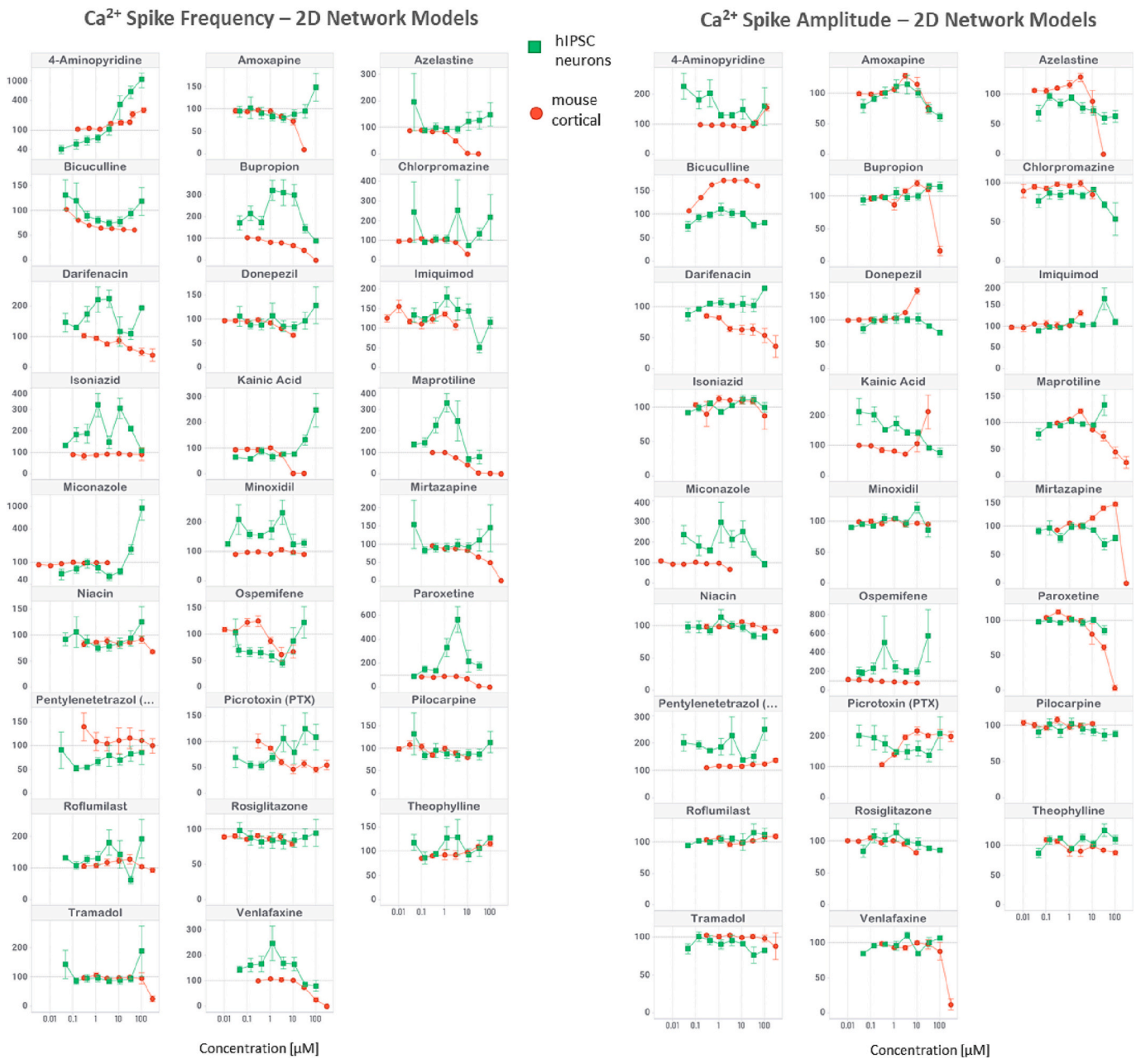

Fig. 9. Comparison of Ca^{2+} oscillation responses to NeuroDeRisk compounds of 2D Networks of hiPSC neurons and of mouse cortical neurons.
Plots of concentration-response curves of Ca^{2+} oscillation frequency (left panel) and amplitude (right panel) to NeuroDeRisk compound set. 2D Network responses of hiPSC Neurons (filled squares, green, ■) and mouse cortical neurons (filled circles, red,●) (n ≥ 6 wells, mean ± SEM).

encoded Ca^{2+} indicators targeted specifically to astrocytes could help identify to what extent if any the observed Ca^{2+} signal arises from astrocytes.(Lohr et al., 2021) However, it is unlikely that the pharmacological responses of the network could be dictated by astrocytes as they lack the excitability and the molecular machinery that creates the complex, pharmacologically responsive Ca^{2+} signaling repertoire of neurons.

The assignment of high seizure risk to a clinical compound based on pharmacovigilance reporting could be biased by pharmacokinetic factors that predispose a certain drug to reach supratherapeutic concentrations in the brain. It is therefore important to note that 9 of the 12 compounds in the FAERS positive category are targeted to the brain and readily cross the blood brain barrier (Table 1). Six of these are antidepressants with synaptic modulation as mechanism of action, and all reduced Ca^{2+} oscillation frequency up to complete cessation in the mouse cortical and neurospheroid models (Table 2, Fig. 7) at higher concentrations. In contrast, none of the FAERS negative drugs are targeted to the brain. Even so, Azelastine, Ospemifene, Valdecoxib, and Roflumilast readily cross the blood brain barrier and Azelastine and Ospemifene were false positives based on reduction of frequency and amplitude in both the neurospheroid and mouse cortical neuron models. These results underscore the limitations of the contingency analysis in the absence of the consideration of the high exposure margins that may have been reached relative to clinically achievable brain concentrations for FAERS compounds. A more thorough assessment would need to take into account understanding of brain penetrance and pharmacokinetics of each compound in the clinical setting. Flagging of a compound via FAERS reporting, unfortunately does not reveal the complete context or circumstances under which the event occurred, and information is thus limited. Assessment may also benefit from more refined analysis of other

Table 2
Ca^{2+} oscillation assessment of hiPSC 2D and 3D network models – comparison to 2D Mouse Cortical (CTX) network.

	Compound	2D hiPSC FREQUENCY	3D hiPSC Neurospheroid FREQUENCY @ 2 hrs	2D Mouse CTX FREQUENCY	2D hiPSC AMPLITUDE	3D hiPSC Neurospheroid AMPLITUDE @ 2 hrs	2D Mouse CTX AMPLITUDE
TOOL	4-AP	+1	+1	+1	+1	-1	+1
	AMOXAPINE	+1	-1	-1	-1	-1	-1
	BICCUCULINE	-1	0	-1	-1	-1	+1
	CHLOPROMAZINE	+1	-1	-1	-1	-1	-1
	DONEPEZIL	-1	-1	-1	-1	-1	+1
	KAINIC ACID	+1	-1	-1	+1	-1	+1
	PENTYLENETERAZOLE	-1	0	0	+1	-1	+1
	PICROTOXIN	-1	0	-1	+1	+1	+1
	PILOCARPINE	-1	-1	-1	-1	+1	0
	SNC-80	ND	-1	ND	ND	-1	ND
	STRYCHNINE	ND	0	ND	ND	0	ND
FAERS Positive	AMITRIPTYLINE	ND	-1	ND	ND	0	ND
	BUPROPION	+1	-1	-1	0	-1	-1
	CLOZAPINE	ND	-1	ND	ND	-1	ND
	DIPHENHYDRAMINE	ND	-1	ND	ND	-1	ND
	ISONAZID	+1	0	0	0	0	0
	MAPROTILINE	+1	-1	-1	-1	-1	-1
	MIRTAZAPINE	0	-1	-1	-1	-1	-1
	PAROXETINE	+1	-1	-1	-1	-1	-1
	TEMOZOLOMIDE	ND	0	ND	ND	0	ND
	THEOPHYLLINE	+1	+1	+1	+1	-1	-1
	TRAMADOL	+1	+1	-1	-1	-1	-1
	VENLAFAXINE	+1	-1	-1	-1	-1	-1
FAERS Negative	AZELASTINE	+1	-1	-1	-1	-1	-1
	DARIFENACIN	+1	-1	-1	+1	-1	-1
	IMIQUIMOD	+1	+1	+1	+1	-1	+1
	MICONAZOLE	+1	+1	0	+1	-1	-1
	MINOXIDIL	+1	0	0	0	0	0
	NIACIN	-1	0	-1	-1	0	0
	OSPEMIFENE	-1	-1	-1	+1	-1	-1
	ROFLUMILAST	+1	+1	0	0	-1	0
	ROSIGLITAZONE	-1	-1	-1	-1	0	-1
	VALDECOXIB	ND	+1	ND	ND	-1	ND
ALL COMPOUNDS	Assay Comparisons:	FREQUENCY			AMPLITUDE		
	2D Matches to 3D Results:	2 D hiPSC FCDI 10 out of 26 (38%)		2D Mouse CTX 20 out of 26 (77%)	2 D hiPSC FCDI 13 out of 26 (50%)		2D Mouse CTX 17 out 26 (65%)
	2D Matching Results:	10 out of 26 (38%)			17 out of 26 (65%)		
	ND: compound was not tested due to either association with health hazard/toxicity or lack of availability						

Table of Directional Effects on Ca^{2+} Peak Frequency and Peak Amplitude in Response to NeuroDeRisk Compounds.
(+1), Increase of Parameter; (−1), Decrease of Parameter; (0), Limited if Any Change in Parameter.
Shading Indicates Matching Direction of Parameter Changes in at Least Two Models.

intrinsic drug parameters, and multivariate regression and machine learning approaches to optimization of prediction (Ishibashi et al., 2021; Wang et al., 2022). A previous attempt to classify the epileptogenic potential of marketed drugs has also found that drugs that have access to the brain are more likely to be associated with seizures, as well as the lack of expected clear correlation between dose of the drug and seizure incidence (Ruffmann et al., 2006).

Roflumilast, a PDE4 inhibitor, had a unique effect to increase frequency in both 2D hiPSC and neurospheroid models, decrease amplitude in the neurospheroid model, while leaving the mouse cortical model

Table 3
Determination of parameter change scoring criteria that maximize FAERS seizurogenicity outcome predictivity of each assay.

SCORING Criteria#	Model	FAERS+		FAERS-		Sensitivity	Specificity	PPV	NPV	Accuracy	Youden Index
		TP	FN	TN	FP						
Case 1 POSITIVE = FREQ. OR AMPL. Changes Independent of Direction	hIPSC 3D Spheroids	10	2	2	8	0.83	0.20	0.56	0.50	0.55	0.03
	Mouse cortical 2D	7	1	2	7	0.88	0.22	0.50	0.67	0.53	0.10
	hIPSC 2D	8	0	0	9	1.0	0	0.47	0	0.47	0.0
Case 2 POSITIVE = FREQ. Changes Independent of Direction	hIPSC 3D Spheroids	10	2	2	8	0.83	0.20	0.56	0.50	0.55	0.03
	Mouse cortical 2D	**7**	**1**	**3**	**6**	**0.88**	**0.33**	**0.54**	**0.75**	**0.59**	**0.21**
	hIPSC 2D	7	1	0	9	0.88	0.00	0.44	0.00	0.41	-0.13
Case 3 POSITIVE = Decrease in FREQ.	**hIPSC 3D Spheroids**	**8**	**4**	**6**	**4**	**0.67**	**0.60**	**0.67**	**0.60**	**0.64**	**0.27**
	Mouse cortical 2D	6	2	4	5	0.75	0.44	0.55	0.67	0.59	0.19
	hIPSC 2D	0	8	6	3	0.00	0.67	0.00	0.43	0.35	-0.33
Case 4 POSITIVE = Decrease in FREQ. AND AMPL.	**hIPSC 3D Spheroids**	7	5	7	3	**0.58**	**0.70**	**0.70**	**0.58**	**0.64**	**0.28**
	Mouse cortical 2D	6	2	5	4	**0.75**	**0.56**	**0.60**	**0.71**	**0.65**	**0.31**
	hIPSC 2D	0	8	7	2	0.00	0.78	0.00	0.47	0.41	-0.22
Case 5 POSITIVE = Decrease in AMPL.	**hIPSC 3D Spheroids**	9	3	3	7	0.75	0.30	0.56	0.50	0.55	0.05
	Mouse cortical 2D	7	1	4	5	**0.88**	**0.44**	**0.58**	**0.80**	**0.65**	**0.32**
	hIPSC 2D	5	3	6	3	**0.63**	**0.67**	**0.63**	**0.67**	**0.65**	**0.29**
Case 6 POSITIVE = Increase in FREQ.	**hIPSC 3D Spheroids**	2	10	6	4	0.17	0.60	0.33	0.38	0.36	-0.23
	Mouse cortical 2D	1	7	8	1	0.13	0.89	0.50	0.53	0.53	0.01
	hIPSC 2D	**7**	**1**	**3**	**6**	**0.88**	**0.33**	**0.54**	**0.75**	**0.59**	**0.21**

 # Explanation of Scoring Criteria for Positive Risk Assessment

- **(Case1) Any effect of the compound on either Frequency OR Amplitude parameter, whether to increase or decrease the parameter, is considered a Positive. Lack of an effect in both parameters is considered Negative for ictogenicity.**
- **(Case2) Any effect of the compound on Peak Frequency, whether to increase or decrease the parameter, is considered a Positive**
- **(Case3) Compounds that decrease Peak Frequency, irrespective of effects on Peak Amplitude, are considered a risk for ictogenicity.**
- **(Case4) Compounds that decrease BOTH Peak Frequency AND Peak Amplitude are considered a risk for ictogenicity.**
- **(Case5) Compounds that decrease Peak Amplitude, irrespective of effects on Peak Frequency, are considered a risk for ictogenicity.**
- **(Case6) Compounds that increase Peak Frequency, irrespective of effects on Peak Amplitude, are considered a risk for ictogenicity.**

Scoring of the assays as a tool to predict compound ictogenicity after exposure to a test compound. Number of true positive (TP), false positive (FP), true negative (TN) and false negative (FN) findings using different criteria to determine what constitutes a Positive (P) test result, after presence and directionality of effects on both Ca^{2+} spike Counts and Peak Amplitudes are considered. Sensitivity was calculated as (TP/TP + FN), specificity as (TN/TN + FP), predictive positive value (PPV) as (TP/TP + FP), negative predictive value NPV as (TN/TN + FN), Accuracy as (TP + TN)/(TP + FP + TN + FN), and Youden index as (sensitivity + specificity)-1. Only FAERS+ and FAERS- results, without consideration of Tool Compounds, were used to optimize predictivity.
Colored conditions highlight conditions where Youden Indexes are elevated.

unaffected. While originally developed for chronic obstructive pulmonary disease, Roflumilast has recently been investigated for its potential as a cognitive enhancer in clinical trials (Blokland et al., 2019). The divergent responses between the mouse and hiPSC derived models underscore the utility of testing compounds directly in human models that are likely to yield better translational insight into fundamental mechanisms of modulation that may be observed clinically. In this context, the distinction between detecting a potentially useful pharmacological effect of a compound in the network model, such as is observed for Roflumilast, or ascribing potential toxicity, becomes a challenge that requires further refinement of understanding of these models for risk-benefit assessment. Our assays do not distinguish between functional

effects of compounds based on general cellular toxicity versus functional modulation that may underlie changes to frequency or amplitude of the Ca^{2+} oscillation. Additional endpoints of cell health and mitochondrial viability would no doubt help to refine the interpretation of the functional changes observed (Sirenko et al., 2019; Wang et al., 2022). In addition, a more refined multi-parametric analysis of Ca^{2+} peak shapes, amplitude histograms, peak clustering, and interpeak interval variability may provide additional insight and information upon which to distinguish and classify compound effects.

Another finding of this study was that the concentration-response curves of amplitude and frequency for the mouse cortical and neurospheroid models were mostly graded with concentration (Figs. 6–8), suggesting good reproducibility of responses from well to well at a given test concentration. When comparing the 2D network results from mouse cortical and hiPSC neurons (Fig. 9), however, the hiPSC 2D network responses show more variability with concentration. This variability in concentration-responses has also been observed in MEA studies of hiPSC neuron 2D networks that are matured over a short 2 to 3 week period (see accompanying NeuroDeRisk MEA study in this issue). Connectivity of neurons may not be homogeneous from well to well given the much shorter network maturation time allotted to the 2D hiPSC model (22–24 days) in comparison with the 3D hiPSC neurospheroids (84–87 days). Another point of consideration is potential differences in composition of the neuronal subtypes (Glutamatergic and GABAergic) and their ratio with the glial cells (astrocytes) across the three neuronal models, and how these differences may affect compound responses within the calcium assay.

The variability in the 2D hiPSC network model may also arise from the limited assay optimization time given study timelines in comparison to the 3D neurospheroids which had been optimized for commercial purposes. A recent study with 2D and 3D networks obtained using the same source of hiPSC neuroprogenitor cells cultured for comparable durations has also noted differences in Ca^{2+} responses to test compounds between the two types of networks (Slavin et al., 2021). In addition, it has been reported that hiPSC 3D cultures result in longer neurite outgrowths compared to 2D networks (Chandrasekaran et al., 2017). While neonatal mouse cortical neurons were allowed to establish network connections for 15–17 days after plating, the much shorter gestation and maturation timeline for mouse over human brains may favor a more thorough network establishment in the rodent model (Iwata et al., 2023). Given the role for astrocytes in maturation of network responses, the limited time for astrocytic maturation in the hIPSC 2D network may be another factor contributing to the discrepancies between the 2D and 3D hIPSC derived models.

5. Conclusion

The hiPSC derived network models tested provide novel assay substrates for network level assessment of human receptor based neural activity. The tightly controlled size of neurospheroids and their basal Ca^{2+} spiking responses make the neurospheroid model an ideal substrate for higher throughput plate-based Ca^{2+} flux assays with which the effects of drugs can be evaluated. Similar results were obtained across test platforms and test sites suggesting that the neurospheroid platform is robust, stable, and reproducible in its Ca^{2+} responses. The concordance of responses between mouse primary cortical and 3D hiPSC neural network responses reported here supports the cortical nature of neurospheroid responses. Further optimization of network maturation time may benefit reproducibility of the 2D hiPSC model. None of the three models was able to provide a consistent phenotypic directional response of Ca^{2+} transient changes to well-established tool compounds that evoke seizures (Table 2, Tool Compounds). While it is generally agreed that the brain slice assay is the gold-standard in vitro model for seizurogenicity testing (Zhai, Zhou, & Lagrutta, 2021), the brain slice assay depends on evoked rather than spontaneous activity. In this regard the spontaneous activity that is being modulated in the Ca^{2+} transient assay may not be expected to provide a consistent directional response and may reflect the varied mechanisms of action of the test compounds on synaptic and cell physiology. Therefore these models may have a larger range of applicability not restricted to ictogenicity. A clear advantage of the hIPSC models is that the human molecular pharmacology should outperform non-human models of molecular synaptic physiology. The relative high sensitivity of these assays can make them useful for determining threshold concentrations for functional effects of potentially neuroactive compounds. These thresholds may then inform on efficacy and safety consideration for further compound development. The simplicity and reproducibility of Ca^{2+} oscillation readouts support further investigation of hiPSC derived neuronal sources and their 2- and 3-dimensional networks for neuropharmacological safety screening.

NeuroDerisk project information

The NeuroDeRisk consortium has received funding from the Innovative Medicines Initiative 2 Joint Undertaking under grant agreement No 821528. This Joint Undertaking receives support from the European Union's Horizon 2020 research and innovation program, and EFPIA.

Declaration of Competing Interest

The authors are employees of their respective companies and confirm that there are no known conflicts of interest associated with this publication and there has been no significant financial support for this work that could have influenced its outcome. Mention of trade names or commercial products does not constitute endorsement or recommendation for use.

Data availability

Data will be made available on request.

References

Ali, F., & Kwan, A. C. (2020). Interpreting in vivo calcium signals from neuronal cell bodies, axons, and dendrites: A review. *Neurophotonics, 7*, 11402.

Andronis, C., Silva, J. P., Lekka, E., Virvilis, V., Carmo, H., Bampali, K., … Savic, M. M. (2020). Molecular basis of mood and cognitive adverse events elucidated via a combination of pharmacovigilance data mining and functional enrichment analysis. *Archives of Toxicology, 94*, 2829–2845.

Blokland, A., Van Duinen, M. A., Sambeth, A., Heckman, P. R. A., Tsai, M., Lahu, G., … Prickaerts, J. (2019). Acute treatment with the PDE4 inhibitor roflumilast improves verbal word memory in healthy old individuals: A double-blind placebo-controlled study. *Neurobiology of Aging, 77*, 37–43.

Boutin, M. E., Strong, C. E., Van Hese, B., Hu, X., Itkin, Z., Chen, Y. C., LaCroix, A., Gordon, R., Guicherit, O., Carromeu, C., Kundu, S., Lee, E., & Ferrer, M. (2022). A multiparametric calcium signal screening platform using iPSC-derived cortical neural spheroids. *SLAS Discovery, 27*, 209–218.

Bradley, J. A., Luithardt, H. H., Metea, M. R., & Strock, C. J. (2018). In vitro screening for seizure liability using microelectrode array technology. *Toxicological Sciences, 163*, 240–253.

Bryant, S. D., Ibis, G., Seidel, T., Kohlbacher, S., Heider, J., Ernst, M., … Langer, T. (2022). The NeuroDeRisk toolbox: DeRisking chemical structures for neurotoxic adverse outcomes. *Toxicology Letters, 368*, S82.

Chandrasekaran, A., Avci, H. X., Ochalek, A., Rosingh, L. N., Molnar, K., Laszlo, L., … Dinnyes, A. (2017). Comparison of 2D and 3D neural induction methods for the generation of neural progenitor cells from human induced pluripotent stem cells. *Stem Cell Research, 25*, 139–151.

Costa, V., Aigner, S., Vukcevic, M., Sauter, E., Behr, K., Ebeling, M., … Jagasia, R. (2016). mTORC1 inhibition corrects neurodevelopmental and synaptic alterations in a human stem cell model of tuberous sclerosis. *Cell Reports, 15*, 86–95.

Dalgin, G., Tryba, A. K., Cohen, A. P., Park, S. Y., Philipson, L. H., Greeley, S. A. W., & Garcia, A. J. (2021). Developmental defects and impaired network excitability in a cerebral organoid model of KCNJ11 p.V59M-related neonatal diabetes. *Scientific Reports, 11*, 21590.

Dravid, S. M., & Murray, T. F. (2004). Spontaneous synchronized calcium oscillations in neocortical neurons in the presence of physiological [Mg^{2+}]: Involvement of AMPA/kainate and metabotropic glutamate receptors. *Brain Research, 1006*, 8–17.

Easter, A., Bell, M. E., Damewood, J. R., Jr., Redfern, W. S., Valentin, J. P., Winter, M. J., … Bialecki, R. A. (2009). Approaches to seizure risk assessment in preclinical drug discovery. *Drug Discovery Today, 14*, 876–884.

Gao, M., Igata, H., Takeuchi, A., Sato, K., & Ikegaya, Y. (2017). Machine learning-based prediction of adverse drug effects: An example of seizure-inducing compounds. *Journal of Pharmacological Sciences, 133*, 70–78.

Ishibashi, Y., Odawara, A., Kinoshita, K., Okamura, A., Shirakawa, T., & Suzuki, I. (2021). Principal component analysis to distinguish seizure liability of drugs in human iPS cell-derived neurons. *Toxicological Sciences, 184*, 265–275.

Ishii, M. N., Yamamoto, K., Shoji, M., Asami, A., & Kawamata, Y. (2017). Human induced pluripotent stem cell (hiPSC)-derived neurons respond to convulsant drugs when co-cultured with hiPSC-derived astrocytes. *Toxicology, 389*, 130–138.

Iwata, R., Casimir, P., Erkol, E., Boubakar, L., Planque, M., Gallego Lopez, I. M., … Vanderhaeghen, P. (2023). Mitochondria metabolism sets the species-specific tempo of neuronal development. *Science, 379*, eabn4705.

Javaid, M. S., Tan, T., Dvir, N., Anderson, A., O'Brien, T. J., Kwan, P., & Antonic-Baker, A. (2022). Human in vitro models of epilepsy using embryonic and induced pluripotent stem cells. *Cells-Basel., 11*.

Kamioka, H., Maeda, E., Jimbo, Y., Robinson, H. P. C., & Kawana, A. (1996). Spontaneous periodic synchronized bursting during formation of mature patterns of connections in cortical cultures. *Neuroscience Letters, 206*, 109–112.

Koseki, N., Deguchi, J., Yamashita, A., Miyawaki, I., & Funabashi, H. (2014). Establishment of a novel experimental protocol for drug-induced seizure liability screening based on a locomotor activity assay in zebrafish. *The Journal of Toxicological Sciences, 39*, 579–600.

Kuijlaars, J., Oyelami, T., Diels, A., Rohrbacher, J., Versweyveld, S., Meneghello, G., … Verheyen, A. (2016). Sustained synchronized neuronal network activity in a human astrocyte co-culture system. *Scientific Reports, 6*, 36529.

Kumlien, E., & Lundberg, P. O. (2010). Seizure risk associated with neuroactive drugs: Data from the WHO adverse drug reactions database. *Seizure, 19*, 69–73.

Kundu, S., Boutin, M. E., Strong, C. E., Voss, T., & Ferrer, M. (2022). High throughput 3D gel-based neural organotypic model for cellular assays using fluorescence biosensors. *Communications Biology, 5*, 1236.

Levesque, M., & Avoli, M. (2013). The kainic acid model of temporal lobe epilepsy. *Neuroscience and Biobehavioral Reviews, 37*, 2887–2899.

Lohr, C., Beiersdorfer, A., Fischer, T., Hirnet, D., Rotermund, N., Sauer, J., … Gee, C. E. (2021). Using genetically encoded calcium indicators to study astrocyte physiology: A field guide. *Frontiers in Cellular Neuroscience, 15*, Article 690147.

Marchetto, M. C., Carromeu, C., Acab, A., Yu, D., Yeo, G. W., Mu, Y., … Muotri, A. R. (2010). A model for neural development and treatment of Rett syndrome using human induced pluripotent stem cells. *Cell, 143*, 527–539.

Murphy, T. H., Blatter, L. A., Wier, W. G., & Baraban, J. M. (1992). Spontaneous synchronous synaptic calcium transients in cultured cortical-neurons. *The Journal of Neuroscience, 12*, 4834–4845.

NeuroDeRisk. (2019). NeuroDeRisk: Neurotoxicity de-risking in preclinical drug discovery. https://www.imi.europa.eu/projects-results/project-factsheets/neuroderisk. online.

Nieto-Estevez, V., & Hsieh, J. (2020). Human brain organoid models of developmental epilepsies. *Epilepsy Currents, 20*, 282–290.

Odawara, A., Katoh, H., Matsuda, N., & Suzuki, I. (2016). Physiological maturation and drug responses of human induced pluripotent stem cell-derived cortical neuronal networks in long-term culture. *Scientific Reports, 6*, 26181.

Pacico, N., & Meur, A. M. L. (2013). New in vitro phenotypic assays for epilepsy: Fluorescent measurement of synchronized neuronal calcium oscillations. *Epilepsia, 54*, 45.

Pacico, N., & Mingorance-Le Meur, A. (2014). New in vitro phenotypic assay for epilepsy: Fluorescent measurement of synchronized neuronal calcium oscillations. *PLoS One, 9*, e84755.

Richards, G. R., Jack, A. D., Platts, A., & Simpson, P. B. (2006). Measurement and analysis of calcium signaling in heterogeneous cell cultures. *Methods in Enzymology, 414*, 335–347.

Rockley, K. L., Roberts, R. A., & Morton, M. J. (2019). Innovative models for in vitro detection of seizure. *Toxicology Research, 8*, 784–788.

Roussignol, G., Peladan, J., Essner, E., Falga, A., Demuynck, A., Bethencourt, M., … Meot, F. (2017). Neuronal calcium oscillations for preclinical seizure risk evaluation. *Journal of Pharmacological and Toxicological Methods, 88*, 232.

Ruffmann, C., Bogliun, G., & Beghi, E. (2006). Epileptogenic drugs: A systematic review. *Expert Review of Neurotherapeutics, 6*, 575–589.

Shirakawa, T., & Suzuki, I. (2020). Approach to neurotoxicity using human iPSC neurons: Consortium for safety assessment using human iPS cells. *Current Pharmaceutical Biotechnology, 21*, 780–786.

Sirenko, O., Parham, F., Dea, S., Sodhi, N., Biesmans, S., Mora-Castilla, S., … Carromeu, C. (2019). Functional and mechanistic neurotoxicity profiling using human iPSC-derived neural 3D cultures. *Toxicological Sciences, 167*, 58–76.

Slavin, I., Dea, S., Arunkumar, P., Sodhi, N., Montefusco, S., Siqueira-Neto, J., … Carromeu, C. (2021). Human iPSC-derived 2D and 3D platforms for rapidly assessing developmental, functional, and terminal toxicities in neural cells. *International Journal of Molecular Sciences, 22*, 1908.

Strickland, J. D., Martin, M. T., Richard, A. M., Houck, K. A., & Shafer, T. J. (2018). Screening the ToxCast phase II libraries for alterations in network function using cortical neurons grown on multi-well microelectrode array (mwMEA) plates. *Archives of Toxicology, 92*, 487–500.

Strong, C.E., Kundu, S., Boutin, M., Chen, Y.-C., Wilson, K., Lee, E., & Ferrer, M. (2022). Functional brain region-specific neural spheroids for modeling neurological diseases and therapeutics screening. bioRxiv, 2022.05.04, 490442.

Sundberg, M., Tochitsky, I., Buchholz, D. E., Winden, K., Kujala, V., Kapur, K., … Sahin, M. (2018). Purkinje cells derived from TSC patients display hypoexcitability and synaptic deficits associated with reduced FMRP levels and reversed by rapamycin. *Molecular Psychiatry, 23*, 2167–2183.

Tidball, A. M., & Parent, J. M. (2016). Concise review: Exciting cells: Modeling genetic epilepsies with patient-derived induced pluripotent stem cells. *Stem Cells, 34*, 27–33.

Tukker, A. M., Wijnolts, F. M. J., de Groot, A., & Westerink, R. H. S. (2020). Applicability of hiPSC-derived neuronal cocultures and rodent primary cortical cultures for in vitro seizure Liabiliy assessment. *Toxicological Sciences, 178*, 71–87.

Wang, Q., Cohen, J. D., Yukawa, T., Estrella, H., Leonard, C., Nunes, J., … Wagoner, M. P. (2022). Assessment of a 3D neural spheroid model to detect pharmaceutical-induced neurotoxicity. *ALTEX-Alternatives to Animal Experimentation, 39*, 560–582.

Wang, X. S., & Gruenstein, E. I. (1997). Mechanism of synchronized Ca^{2+} oscillations in cortical neurons. *Brain Research, 767*, 239–249.

Winter, M. J., Redfern, W. S., Hayfield, A. J., Owen, S. F., Valentin, J. P., & Hutchinson, T. H. (2008). Validation of a larval zebrafish locomotor assay for assessing the seizure liability of early-stage development drugs. *Journal of Pharmacological and Toxicological Methods, 57*, 176–187.

Woodruff, G., Phillips, N., Carromeu, C., Guicherit, O., White, A., Johnson, M., … Harrington, A. W. (2020). Screening for modulators of neural network activity in 3D human iPSC-derived cortical spheroids. *PLoS One, 15*, Article e0240991.

Yokoi, R., Shigemoto-Kuroda, T., Matsuda, N., Odawara, A., & Suzuki, I. (2022). Electrophysiological responses to seizurogenic compounds dependent on E/I balance in human iPSC-derived cortical neural networks. *Journal of Pharmacological Sciences, 148*, 267–278.

Youden, W. J. (1950). Index for rating diagnostic tests. *Cancer, 3*, 32–35.

Zhai, J., Zhou, Y. Y., & Lagrutta, A. (2021). Sensitivity, specificity and limitation of in vitro hippocampal slice and neuron-based assays for assessment of drug-induced seizure liability. *Toxicology and Applied Pharmacology, 430*, Article 115725.